Reply to referee 1

We thank the referee for the comprehensive and constructive review. All aspects have been addressed in a revised manuscript and a new supplement. Below please find our point-by-point reply to the comments.

> This paper entitled "Revised mineral dust emissions in the atmospheric chemistry-climate model EMAC (based on MESSy 2.52)" and submitted to GMD presents new developments concerning the parameterization of dust emissions in the global model ECHAM/MESSy. These new developments have been evaluated and compared to the previous version of the model in terms of the resulting aerosol optical depth. The use of ground-based (AERONET) and satellite (MODIS, IASI) has shown the improvement brought by this new version. This paper is therefore interesting for the community working on dust modeling, and the manuscript is well written. However, the current version needs major revision before considering the publication in GMD because of the following points:
>
> - The evaluation of the revised emissions is limited to the aerosol optical depth, which is not enough to estimate the quality of the parameterization. AOD is indeed a relevant parameter to evaluate the integrated effect of dust aerosols on radiation, but it can hinder some compensating errors. Besides, such parameters as the dust size distribution, the dust vertical profile or dust deposition are essential for radiative budget and effects on climate, and are not constrained by AOD. The authors could for example add an evaluation of surface concentrations, dust deposition, dust emission fluxes or dust vertical profiles, as done by similar recent studies (Kok et al., 2014; Albani et al., 2014; Klose et al., 2014; Gherboudj et al., 2015).

We appreciate the advice and have added the evaluation of surface concentrations and dust deposition for an even more comprehensive validation. Regarding the current evaluation we would like to point out that our comparison with the satellite retrieved 10 um DAOD goes beyond the evaluation used in other studies and, combined with the AOD comparison at visible wavelengths, amongst others probes aspects of the particle size distribution.

> - As there are many papers on dust modeling, the authors should highlight more the originality of their work. In this purpose, they should add a paragraph in the introduction presenting the state-of-the-art in dust modeling in global chemistry-climate models. This would be useful for the whole community, and would not restrain the impact of the paper to the ECHAM community as it could be the case with the current version of the paper.

We have extended the introduction accordingly.

> Specific comments:
>
> - Abstract: The authors mention several times the possibility to run high resolution simulations. What is the targeted resolution? Do the scheme need any modification for this high resolution?

The upper limit of the target resolution is given by the resolution of the updated input data. The target will be T255 (about 0.5 degree at the equator) or higher (which so far is only mentioned in the conclusions). With at least 0.1 degree resolution, the new input data will also serve considerably higher resolving simulations. Also the emission scheme itself can be used straight forwardly at higher resolution. As it is not entirely resolution independent the overall scaling might need to be adjusted. We have added the following sentence to the introduction:

Page 2, line 29 "To equip the model for simulations at resolution T255 (about 0.5 degree) or higher, new input data should have at least 0.1 degree resolution."

And in section 3:

Page 6, line 7 "When switching to different model resolutions, the scaling factor can be used to balance potential resolution dependencies of the emission scheme."

> - Page 2 Lines 18-19: The authors should justify the "rapid changes of deserts and semi-arid regions in recent decades"

References to Figs. 1 and 2 and literature have been included.

- Page 3 Section 2.1: Looking at Fig.1, I get the impression that there are more regions with shrinking deserts, is it true?

That is correct, the area with positive correlation coefficient covers $1.3 \cdot 10^6$ km^2 globally which is about half the area with negative correlation coefficient ($2.6 \cdot 10^6$ km^2). Additionally, the regions of shrinking deserts are spread over a larger area because they are predominantly surrounding the large deserts whereas expanding source areas are located more centrally. We have added the numbers to the text.

- Page 3 Line 27: Any justification for the equation (1) giving the vegetation factor? Is it used in other models?

The vegetation factor is the same as used by Astitha et al. 2012 and interpolates linearly between full emissions for no vegetation and entirely suppressed emissions for LAI > 0.35; the threshold value was introduced by Mahowald et al. 1999. We have added the references.

- Page 3 Lines 29-30: Could the authors clarify which statistical test they have used?

The trend has been calculated for each pixel by fitting a linear regression model to the time series of annual average LAI values using least squares. The resulting slope yields the trend and is considered significant (i.e., it is plotted in Fig. 2) if the corresponding p value is below the significance level of 0.05. We have rephrased the sentence.

- Page 4 Section 2.3: Contrary to Sections 2.1 and 2.2, the authors have not elaborated on the differences between the two versions of the clay fraction maps. Which is the expected impact on dust emissions?

The two versions of the clay fractions are now compared in Figure S1 in supplement. The impact on the dust emissions is discussed in the new section 4. The expected impact of the new data is a better representation of details below the 1 degree resolution such as river valleys. Moreover, as mentioned, the new data is more appropriate to represent the relevant topmost soil layer. As the clay fraction map is assumed to be static (based on the longer typical time-scales of the relevant geological processes), unlike in Sect. 2.1 and 2.2 we could not perform trend and variation analysis.

- Page 4 Lines 26-29: Is there any work forecast to include again the effect of soil moisture on dust emissions? It might be important in some regions like Sahel.

We agree that the effect of soil moisture is important in regions like the Sahel (or the Middle East) and it would be very desirable to consider it in the model. A prerequisite would be a soil model more detailed than the current bucket model to obtain soil moisture values for only the topmost surface layer. While the inclusion of new soil models in EMAC is discussed, to our knowledge one has yet to be implemented.

- Page 5 Line 5: This equation differs from the one given in Astitha et al. (2012), the authors should correct it or explain why it is different.

Eq. (9) used by Astitha et al. (2012) implies that the horizontal flux H is proportional to

$$\begin{aligned} u_*^3(1+u_{*t}/u_*)(1-u_{*t}^2/u_*^2) &= u_*^3(1+u_{*t}/u_*)(1+u_{*t}/u_*)(1-u_{*t}/u_*) \\ &= (u_*+u_{*t})(u_*+u_{*t})(u_*-u_{*t}) \end{aligned}$$

which agrees with the RHS of our Eq. (2).

- Page 5 Line 9: The authors should justify the choice of 0.4 m/s, and clarify what they call "good results" explaining what has been compared.

The value is justified by the results presented in Sect. 4 which are good in the sense that the validation simulation produces, compared to observations, significantly more realistic results (in terms of skill scores and correlation coefficients) than the reference simulation using the original emission scheme of Astitha et al. (2012)

which already proofed to yield realistic results in other studies. We have added results from simulations using different limits in the supplement (Figure S3).

- Page 5 Line 29: The parameter dmax could be added in Table 2

Dmax has been added to the table.

- Page 6 Lines 10-15: I did not understand if finally the chemical composition of dust is included or not in the model.

As mentioned on Page 6, lines 31f the chemical composition is included in the model for both, reference and validation run. As the corresponding changes to the dust emission scheme are independent of all other modifications, do not affect total dust emission flux and can be used with the original and the revised emission scheme, their effects (see Karydis et al. 2016) have been excluded from the evaluation, but code and data are released with the revision presented here.

- Page 6 Lines 19-21: The list of submodels is unclear for readers not familiar to the model. The authors should add a reference to have the details about these parameterizations.

We have added a reference (http://www.messy-interface.org/current/auto/messy_submodels.html).

- Page 6 Line 25: What is the Tanré climatology used for? (AOD or only other optical properties?)

It is used for extinction, single scattering albedo and asymmetry factor (now mentioned in the text).

- Page 6 Line 30: A reference to Table 1 should be added to present the simulations.

The reference has been added.

- Page 6 Line 32: Is a one-year simulation long enough to evaluate the revised dust emissions? Is there any reason to select the year 2011?

While longer simulations are preferable, the one-year period suffices to yield statistically significant differences between reference and validation simulation and has been chosen considering the computationally expensive model setup used. The year 2011 has been selected to represent a recent period well past the time period on which the old, outdated input data is based on, and to allow to continue the simulation within the period of available new input data in case this would have been necessary to collect more statistics.

- Page 7 Line 15: Which level of AERONET AOD has been used in this comparison?

Level 2 data has been used (now mentioned in the text).

- Page 7 Line 17: Maybe the authors should divide the region B in two sub-regions, for the reader to identify more easily the different stations.

We have divided the region into a northern and southern part.

- Page 7 Lines 29-30: I don't understand how this skill score based on correlation can be affected by a bias.

The overestimation of the AOD during dust events results in an overestimated amplitude of the AOD variation between dust-free (when both reference and validation simulation yield AODs close to zero) and dusty periods. Accordingly, variance and standard deviation are overestimated, the latter entering the skill score defined in Eq. (5).

- Page 7 Section 4.1: It could be also useful to add one or two time series in stations where the score has increased.

We have added time series plots of the five stations with the largest increase to the supplement (Fig. S5).

- Page 8 Line 1: Which is the altitude of the model grid cell?

The model grid cell has a surface altitude of 63 m which we now mention in the text.

- Page 8 Line 21: Is this increase of spatial correlation statistically significant?

The statistical error of the numbers is small, the error estimates obtained by jackknife resampling of the more than 10^5 pixel values are 0.004 for the correlation coefficients and 0.006 for the skill scores. Therefore, the digits provided are presumably exact and the probability for the increase under the null hypothesis (assuming no improvement) is virtually zero.

It should be stressed that the improvements reflected by the numbers are substantial and the improvement of the global AOD distribution is a major advantage of the revised emissions.

- Page 8 Lines 28-30: The authors could think about adding a score for the measuring the improvement in seasonal cycle, which could reinforce the robustness of their results.

We have added statistical analysis of the seasonal AOD and DAOD values over the Arabian Peninsula to the supplement (Figs. S6, S7).

- Page 9 Line 17: Same remark for the significance of the increase in the skill score.

Here, the error estimates for the reference results are slightly larger than above (0.012 for the correlation coefficient, 0.017 for the skill score) due to the distinct peaks in the reference DAOD distribution, but still very small compared to the increase due to the revised emissions, therefore again the increases are highly significant.

We apologise that the numbers in the text (page 9, lines 16f) are not the correct numbers provided in the caption of Figure 12. This has been fixed.

- Page 9 Line 32: The time dependence of land cover and vegetation has not been tested here because the simulations were too short.

We agree, however, using the input data based on observations from the year simulated (2011) likely contributed to the more realistic results.

Technical comments:
- Page 2 Lines 8-9: The abbreviations DU_Astitha1 and DU_Astitha2 are useless since they are not used in the rest of the paper.

The abbreviations are the names of the corresponding options in the EMAC setup. To unambiguously specify the emission scheme our study builds on, we would like to keep mentioning the names here.

- Page 6 Line 24: ISORROPIA

The typo has been fixed.

- Figure 1: The color bar should be changed, because the values below -0.2 cannot be distinguished.

The contrast has been increased.

- Figure 8: The authors could replace the letters (A, B, etc.) by the name of the regions in the blue line at the top of the figure.

We have introduced more descriptive abbreviations.

- Figure 9: AERONET data is represented with dots in the figure, while it is a line in the caption.

This has been fixed.

- References: The format needs to be homogenized (notably the use of first names for the first author).

The bibliography has been revised.

Reply to referee 2

We thank the referee for the thorough review and the helpful advices to improve the article. They have all been considered in a revised manuscript and a new supplement. In the following please find our replies to the individual comments.

> General comments This study presents updates of the dust emission scheme implemented in the global atmospheric chemistry model EMAC based on the previous work of Astitha et al. (2012). The land cover, vegetation topography and clay fraction maps are updated to more recent versions using higher spatial resolution. Changes are also imposed to the dust emission scheme directly. The updated dust emissions are evaluated with AOD measurements from AERONET, MODIS and IASI for the year 2011. The title, flow and structure of the paper are appropriate. All updates are well received and long needed, given the importance of quality input data to accurately parameterize physical processes that cannot be described by first principles. However, the authors keep the evaluation part largely on the qualitative side, which does not help the reader and the community to fully understand why these changes were impactful and significant. The conclusions are also very brief for a model development/improvement paper. The authors miss a great opportunity to discuss the very interesting aspects of each revision and inform the community of which one should be considered more impactful (if not all). The specific comments below will help the authors revise the paper so it can be accepted for publication with GMD.

We have added a section discussing the effects of the individual modifications. The evaluation - comparing numeric results for AOD, DAOD, correlation coefficients and skill scores - has been extended by even more quantitative comparisons of dust concentrations and deposition rates.

> Specific comments/suggestions
> Section 2.2 (Vegetation): Please elaborate on the calculation of fveg (Eq.1): What is the role of 0.35 and what is the meaning of fveg being 1 or less than 1.

This vegetation factor, also used by Astitha et al. 2012, interpolates linearly between full emissions for no vegetation and entirely suppressed emissions for LAI > 0.35 which was introduced as threshold by Mahowald et al. 1999. We have added this information.

> Section 2.3 (Clay fraction): provide a map of the updated clay fraction in comparison to the one previously used in the model. It will provide context on the significance of changes that later affect the parameterization scheme.

The map has been added to the supplement.

> Section 3 Page 4 (soil moisture): The soil moisture term in Astitha et al. (2012) and Eq. A1 in this paper is omitted from the threshold friction velocity. However, the authors correctly describe the dependence of dust emission on soil moisture at the end of this paragraph. What is not clear is if the statement "we consider a detailed parametrisation of the soil moisture effect to be essential to capture the observed trends in future simulations. This will require a comprehensive soil model providing accurate moisture values for the topmost surface layer" refers to an action already taken for this study or a future goal. In any case, a discussion on how the exclusion of soil moisture correction influences the simulations is important here.

The more comprehensive soil model is a future goal, we have clarified the statement and added a figure illustrating the effect of omitting the factor to the supplement.

> Page 5, (Surface friction velocity limit): a note must be placed that Eq.2 holds only when $u^* > u^*t$. Also, choosing to limit the threshold velocity to a maximum value of 0.4 m/s seems arbitrary and needs to be elaborated. What led the authors to this specific value? Some context and rationale must be provided.

We have clarified the equation and included results for different limits in the supplement.

> Page 5 (Topography factor): I am not sure of the role of the normalization factor 5.3 and how it conserves global emissions. It sounds like a tuning factor to me, so please elaborate on the role of the factor and the method used to estimate it.

Using the topography factor S_{topo} as given in Eq. (3) has two effects: the desired effect is that it adjusts the spatial distribution of the emissions, but since by definition $0 \leq S_{\text{topo}} \leq 1$ and usually $S_{\text{topo}} < 1$ an undesired side effect is the reduction of the emissions globally. We quantified this reduction in a one month simulation obtaining a ratio between the global emissions without and including the factor S_{topo} of 5.3. Consequently, we include $5.3 \times S_{\text{topo}}$ instead of just S_{topo} and thereby conserve the global emissions. In practice, this normalisation factor can be combined with the empirical scaling factor c, hence it introduces no additional tuning factor. We have expanded the corresponding corresponding text.

> Page 5 (Mode mapping): This is not a strict update of the emission scheme but rather an alteration in order to use the GMXE aerosol model compared to M7 used by Astitha et al. (2012). A brief note must be included in this section to clarify that the original scheme (as well as the reference simulation herein) used a different aerosol module thus a different approach to particle size distribution. The omission of the eight transport size bins is surely a change from the original version.

In this study, we use the GMXE submodel for both, reference and validation simulation. Since GMXE is based on M7 and uses the same modal concept, the question of how to map the three emission modes to the aerosol submodel modes is unaffected by this choice. Since in the original scheme the dust was not further processed while in the "transport" bins but directly mapped to the GMXE/M7 modes, skipping this step is in fact an implementation detail and when aligning the threshold between accumulation and coarse mode with the bin boundary at radius 0.6 um yields identical results.

> Figure 6: what is the higher value in this scale (above 0.1)? When we see 0.1 fraction of Ca++, does that indicate the mass, volume (or else) fraction of the total particles within each specific grid cell? A better explanation of the mineral cations fraction could be included also in page 6 (last paragraph of section 3).

The upper limit of the scale is 0.12, which is reached by the Ca++ fraction in the Kalahari and Taklamakan Desert; we have added a tick mark. The fractions shown in Figure 6 are mass fractions; we have added this missing information in the caption.

> Section 4.1, page 7: 1. "On the other hand, dust events observed by AERONET in January and December are reproduced by the validation simulation, but not by the reference simulation": this comparison is not at all discernible in the plot as it is. If this is an important argument, the plot must be revised somehow to make the statement visible.

We have marked the events we are referring to in the plot.

> 2. Given that Izana and La Laguna are within the same model grid cell, an average of the AOD from both sites could be an alternative way to compare with the model value. In addition, when evaluating numerical model simulations one can employ the nearest neighbor (as done here) or a bilinear interpolation between the observation and the model value from the four closest grid points.

Averaging the AOD values of all stations within the same grid cell generally is a reasonable strategy, in this case, however, even La Laguna station at 568 m altitude is not representative for the grid cell which is mostly covered by ocean. Since the neighbouring cells are also predominantly covered by water, bilinear interpolation would not make a big difference in this regard. Better agreement could be obtained by computing the model AOD at station altitude rather than at model surface height. Generally, such distinctive sub-grid topographies and shore lines reveal the limitations of the model resolution.

> 3. The main criticism I have for the evaluation using the skill score (as with any other statistical metric) is the qualitative determination of which configuration provided the best results. Characterizations such as “slightly better” or “marginally larger” do not show robustness in the performed evaluation. My immediate question is: are these differences statistically significant? Are they statistically different? This is the only way to prove or convince the audience that a, say, 0.05 change in the skill score is significant enough.

Measures like the skill score are supposed to quantify agreement. The significance of the skill score improvement has only been indicated by the dominance of green bars in Figure 8. In the revised manuscript we have amended the figure to depict error estimates for the ΔS values.

> 4. What about using AOD of coarse vs. accumulation modes from AERONET?

The fine/coarse mode AOD product is more sparse than the AOD data, moreover it is only available at 500 nm and we do not have corresponding model output available. We will extend the evaluation to other observables instead (see below).

> 5. How about using total PM concentrations wherever available (and for cases of high dust concentrations) to evaluate model performance? An additional means of quantitative evaluation needs to be included.

The evaluation will be extended by comparisons with dust concentration and deposition data.

> Figure 8: Please consider replacing “Regions A, B,” etc. from the figure with the names of the regions as it is not convenient to go back and forth between Fig. 7 and 8 to identify the regions.‘

A more convenient naming has been introduced.

> Sections 4.2 and 4.3: The scarcity of desert dust concentration measurements is a well-known problem in the modeling community when assessing model and parameterization scheme performances. This is when satellite and remote sensing observations come into play and are important tools of assessment. Nevertheless, leaving the comparison in the qualitative state only, influences the robustness of the conclusions. Looking at the IASI zoomed plots (Fig. 13), I would not immediately say that the validation is better than the reference simulation. They are different and somewhat both incorrect in my view. If the authors presented a quantitative assessment of the performance, there would be no doubt on the comparison. Also, why is the zoomed area over Middle East only? What is the special interest for this specific region? This has to be explained thoroughly so it will not be seen as “cherry picking”.

To guide the eye in Figs. 11 and 13 we have marked the region where we see considerable improvements, which is the Arabian Peninsula including Iraq, Syria and Jordan. To corroborate the improvements, we have evaluted the spatial correlations and skill scores in this region which significantly increase as shown in the new Figs. S6 and S7 in the supplement. The Middle East is of special interest because there the original emission scheme clearly suffered from outdated input data, as mentioned in the introduction. To avoid the impression of cherry picking we now provide seasonal global plots in a supplement.

> Conclusions: the conclusions are quite brief (two sentences in the end of the section). More discussion should be invoked on how the changes influence a better model performance (as long as there is a robust determination of “better” or “worse”). There are very interesting aspects in this study and it would be very useful for the community to understand how the changes that were implemented individually affect dust emissions. I believe that adding such discussion would greatly strengthen the paper.

The conclusions now reflect the additional aspects covered by the revision.

Appendix: There are a couple of things missing in the depiction of the emission flux jemis (Eq A2): 1) I don't see the mass fraction (source to transport bins, M in Eq.4) that should be multiplied in the right side of the equation. 2) In Astitha et al. (2012) they used the relative surface area covered from particles with diameter D (Srel) to calculate the horizontal flux H. Did the authors omit this calculation in their revisions?

The emission flux given in Eq. (A2) is the total emission flux. In the revised manuscript we have multiplied the mass fraction to present the flux for each mode instead. The factor S_{rel} is only utilised in the emission scheme variant DU_Astitha2, not in the scheme DU_Astitha1 used in this study.

Reply to short comment 1

We propose to amend the title to "Revised mineral dust emissions in the atmospheric chemistry-climate model EMAC (MESSy 2.52 DU_Astitha1 KKDU2017 patch)" and will discuss this suggestion with the responsible editor. The pre-formulated lines on the messy interface homepage have been included in the code availability section. The corresponding author acts as point of contact to obtain code and data as long as they are not yet included in an official MESSy release and the common data pools (the code will become part of the official MESSy code as soon as this manuscript is published).

List of relevant changes

Title

The title has been changed to “Revised mineral dust emissions in the atmospheric chemistry-climate model EMAC (MESSy 2.52 DU_Astitha1 KKDU2017 patch)” (addressing short comment 1)

Supplement

A supplementary PDF file comprising 16 new figures has been added

Introduction

The introduction has been expanded by the second and third paragraph (addressing referee comment 1)

Section 4

A new section 4 on the “Effects of the individual modifications” has been added, including the new Figure 7 (addressing referee comment 2)

Section 5.4

A new section 5.4 evaluating “Dust concentration and deposition” has been added, including Figure 15 (addressing referee comment 1)

Conclusions

The conclusions have been expanded

Code and data availability

The “Code and data availability” section has been expanded (addressing short comment 1)

References

Solomos et al., ACPD, 2016 has been updated to Solomos et al. ACP, 2017 and the following references have been added: Albani et al. (2014), Allen et al. (2013), Allen et al. (2015), Dong and Sutton (2015), Gherboudj et al. (2015), Jones et al. (2012), Klose et al. (2014), Kok et al. (2014), Mahowald et al. (1999), Marsham et al. (2013), Pantillon et al. (2015), Pantillon et al. (2016), Pozzer et al. (2015), Shao et al. (2001), Shao et al. (2011)

Figures

Figures 1, 8, 9, 10, 12, 14 (new numbering) have been updated

The following latexdiff output details all changes.

Revised mineral dust emissions in the atmospheric chemistry-climate model EMAC (based on MESSy 2.52 DU_Astitha1 KKDU2017 patch)

Klaus Klingmüller[1], Swen Metzger[2], Mohamed Abdelkader[1,3], Vlassis A. Karydis[1], Georgiy L. Stenchikov[3], Andrea Pozzer[1], and Jos Lelieveld[1,2]

[1]Max Planck Institute for Chemistry, P.O. Box 3060, 55020 Mainz, Germany

[2]The Cyprus Institute, P.O. Box 27456, 1645 Nicosia, Cyprus

[3]King Abdullah University of Science and Technology, Thuwal 23955-6900, Saudi Arabia

Correspondence to: Klaus Klingmüller (k.klingmueller@mpic.de)

Abstract. To improve the aeolian dust budget calculations with the global ECHAM/MESSy atmospheric chemistry-climate model (EMAC) we have implemented new input data and updates of the emission scheme.

The data set comprises landcover classification, vegetation, clay fraction and topography. It is based on up-to-date observations, which is crucial to account for the rapid changes of deserts and semi-arid regions in recent decades. The new Moderate-resolution Imaging Spectroradiometer (MODIS) based landcover and vegetation data is time dependent, and the effect of long-term trends and variability of the relevant parameters is therefore considered by the emission scheme. All input data has a spatial resolution of at least 0.1° compared to 1° in the previous version, equipping the model for high resolution simulations.

We validate the updates by comparing results for the aerosol optical depth (AOD) at 550 nm wavelength from a one year simulation at T106 (about 1.1°) resolution with Aerosol Robotic Network (AERONET) and MODIS observations, and results for the 10 μm dust AOD (DAOD) with Infrared Atmospheric Sounding Interferometer (IASI) retrievals, and dust concentration and deposition results with observations from the AEROCOM dust benchmark data set. The update significantly improves agreement with the observations and is therefore recommended to be used in future simulations.

1 Introduction

Aeolian dust can impair everyday life and air quality especially in severe dust storms. Due to the worldwide presence of dust sources and through long range transport it has a significant global impact on atmospheric radiation transfer and air quality, affecting climate (IPCC, 2014) and human health (Giannadaki et al., 2014), which requires detailed representation in general circulation models (Shao et al., 2011).

~~The global~~ Global models have different requirements regarding the dust emission scheme compared to regional models. As global models require planetary consistent input data sets, the availability of adequate data is more limited. Additionally, the coarser grid spacing requires an appropriate parametrisation of sub-grid processes, and, for example, reproducing individual dust events with global models may have lower priority than adequately representing the atmospheric dust budget on a longer time scale. But with their ever-increasing resolution, global models in many regards correspond to former generation regional models, and therefore established emission schemes are often applied in both, regional and global models.

Global models implement dust emissions with various complexity levels. Even the simplest version, prescribed (*offline*) dust emissions can produce acceptable results for the global aerosol distribution and variability due to the importance of atmospheric transport (Pozzer et al., 2015; Pringle et al., 2010b). Improved agreement with observations is generally achieved with *online* emission schemes which consider actual meteorological conditions, most importantly the surface friction velocity and the wind speed close to the surface. They are combined with a characterisation of surface properties, where properties and relations are to different degrees empirical (*source functions*) or deduced from micro-physical processes. The dominant processes considered are saltation bombardment by sand blasting and aggregate disintegration, and more elaborate emission schemes consider additional effects such as direct aerodynamic entrainment (Shao, 2001; Klose et al., 2014). The inability of most current global models to resolve convection means that haboobs which are responsible for a major fraction of the dust emissions (Marsham et al., 2013; Allen et al., 2013, 2015) are not represented at all. Therefore efforts are made to combine the emission schemes with explicit parametrisations of convective dust storms (Pantillon et al., 2015, 2016).

The global ECHAM/MESSy atmospheric chemistry-climate model (EMAC) (Jöckel et al., 2005, 2010) provides a choice of dust emission schemes (Tegen, 2002; Balkanski et al., 2004; Astitha et al., 2012) to calculate the emission flux online based on the meteorological conditions.

An advanced scheme producing convincing results when compared to observations has been presented by Astitha et al. (2012) building on previous studies (Pérez et al., 2006; Spyrou et al., 2010; Laurent et al., 2008, 2010; Marticorena et al., 1997; Zender et al., 2003; Tegen, 2002), and is the basis of the work presented here. ~~This emission~~ Its basic principles are shared with emission schemes used in many other models (e.g. Zender et al., 2003; Jones et al., 2012; Albani et al., 2014; Huneeus et al., 2011), but alternative approaches exist (e.g. Shao, 2001; Kok et al., 2014). The emission scheme combines meteorological parameters with descriptions of landcover type, clay fraction of the soil and vegetation cover. One variant of the scheme (DU_Astitha2) additionally accounts for regional differences of the particle size distribution, while in the present study we focus on the simpler variant DU_Astitha1, which achieves competitive results with reduced complexity (Astitha et al., 2012) and has proven to perform well in previous studies (Abdelkader et al., 2015, 2016). The emission scheme is summarised in appendix A.

The emission scheme applies physical principles in the sense that the governing equations are derived for microphysical processes that are consistently applied globally without the option to adjust the resulting emissions regionally. In this study we extend the emission scheme by including a topography factor while we strictly adhere to the global consistency concept and refrain from using regional tuning factors.

Though generally the original emission scheme produces convincing results, some shortcomings, predominantly related to the input data, have become apparent recently and are the motivation for the revision presented in this study. The original input data for land cover and vegetation is based on observations from the early 1990s and is thus dated in view of the rapid changes of deserts and semi-arid regions in recent decades ~~.~~(Figs. 1, 2, Klingmüller et al. (2016); Lamchin et al. (2016); Dong and Sutton (2015)). For instance, the emission mask resulting from the land cover data considerably limits emissions in the Middle East, essentially not allowing dust emissions in Syria and northern Iraq. This is in conflict with the emergence of severe dust outbreaks from that region ~~(Solomos et al., 2016)~~(Solomos et al., 2017), and the strong link between the soil conditions in that region and trends of atmospheric dust over the Middle East (Klingmüller et al., 2016). Moreover, only a static land cover map and a single seasonal cycle for the vegetation index was provided.

As a consequence, the effect of variations and trends of these quantities on the modelled dust emissions have been excluded. Further, the resolution of the original input data is limited to $1°$. Particularly for EMAC simulations focusing on dust modelling, high model resolutions are desirable, considering how localised dust outbreaks can occur. In the long term, the resolution of global models will approach the resolution of today's regional models where high resolution input data are essential to include details of dust generation patterns (Shi et al., 2016; Anisimov et al., 2017). For model resolutions higher than T106 ($\approx 1.1°$) as applied in the present study, improved input data is required to justify the numerical effort. To equip the model for simulations at a resolution of T255 ($\approx 0.5°$) or higher, new input data should have at least $0.1°$ degree resolution.

In addition to updated input data addressing these issues, we present adjustments to the emission scheme to assure that the updated input has no undesirable effects such as too strong emissions in mountainous regions and to further improve the performance of the scheme.

To quantify the impact of the updates, we compare a validation simulation with the reference simulation, the latter using the original emission scheme and data. Results and comparisons of other schemes in EMAC are provided elsewhere (Gläser et al., 2012; Astitha et al., 2012). The purpose of the validation is to demonstrate the advantages of the updates and to test the results so that the modifications can swiftly be adopted by the community; more applications and in depth analysis thereof are beyond the scope of this mostly technical study.

The article is structured as follows: in Sect. 2 we introduce and discuss the updated input data; the modifications to the EMAC code are presented in Sect. ~~3.~~ 3 and their individual effects studied in Sec. 4. The effect of both is validated in Sect. ~~4~~ 5 by comparing with the reference simulation, as well as ground based aerosol optical depth (AOD) observations (Sect. ~~4.1~~5.1), and satellite based AOD (Sect. ~~4.2~~5.2) and dust AOD (DAOD) (Sect. ~~4.3) retrievals .~~ 5.3) retrievals as well as concentration and deposition data (Sect. 5.4).

2 Updated input data

2.1 Landcover

To replace the landcover classification map of Olson (1992), we use the MODIS MCD12C1 landcover product (MODIS MCD12C1) at $0.05°$ resolution, allowing for dust emissions from regions classified as *barren or sparsely vegetated*. Not only the resolution is higher than for the Olson data, which in the original emission scheme has been used at $1°$ latitude and longitude (aggregated from $10'$), but also yearly updated data from 2001 to 2012 are provided, also expecting more recent updates to become available. Therefore, changes of the landcover for example due to desertification are taken into account, which have not been considered previously. To assess these changes, we compute for each pixel the Kendall rank correlation coefficient τ of annual mask value, which can be either 0 (non-emitting) or 1 (emitting), and time; the result is shown in Fig. 1. Positive values of τ indicate an expansion of source regions to the respective pixel, negative values a disappearance of sources. In some regions the deserts are shrinking, e.g. in the Sahel, Central Asia and Australia. Expanding source areas are found rather centrally in the dust belt, e.g. in the Sahara, on both sides of the Red Sea and north of the Arabian Peninsula in Syria and Iraq. Globally, the area with positive correlation coefficients covers $1.3 \cdot 10^6\ \mathrm{km}^2$ which is about half the area with negative correlation coefficient ($2.6 \cdot 10^6\ \mathrm{km}^2$). Additionally, the regions of shrinking deserts are spread over a larger area because unlike the centrally located expanding source regions they are predominantly surrounding the large deserts.

2.2 Vegetation

Yuan et al. (2011) have reprocessed the MODIS leaf area index (LAI) products to provide a temporally continuous and spatially consistent LAI data set for climate modelling that encompasses the time period since 2000. We have aggregated this data from 30" to $0.1°$ spatial resolution and from eight-day to one month temporal resolution. The data replaces the twelve month seasonal cycle of the vegetation area index with $1°$ resolution based on the work of Kergoat et al. (1999) and Bonan et al. (2002). Using continually updated monthly values instead of a repeating seasonal cycle implies that multi-annual vegetation trends are taken into account.

The LAI data is used to compute the vegetation factor (Astitha et al., 2012),

$$f_{\mathrm{veg}} = 1 - \frac{\min(\mathrm{LAI}, 0.35)}{0.35}. \quad (1)$$

which linearly interpolates between full emissions for no vegetation and entirely suppressed emissions for $\mathrm{LAI} \geq 0.35$ which was introduced as threshold by Mahowald et al. (1999). The 16 year average, standard deviation of the yearly averages and the trend of the vegetation factor are shown in Fig. 2. The trend has been ~~calulated based on~~ calculated as slope of a linear regression model fitted to the annual averages using ~~linear regression~~least squares; only pixels with p values below the significance level of 0.05 are plotted. As demonstrated by the standard deviation plot, large variability and trends, e.g. related to changing desert boundaries, coincident with the regions of landcover changes, as shown in Fig. 1 can strongly influence the results. The strongest variability is observed in the interior lowlands of Australia (Simpson, Strzelecki and Tirari Deserts), the Thar Desert

(India/Pakistan) and Mesopotamia. While in Australia the variability does not yield a significant trend over the 16 year period, in and around the Thar desert a strong decrease of the vegetation factor, indicating vegetation growth, is observed. This inhibits dust emissions and could result in the significant negative AOD trend in that region reported by Klingmüller et al. (2016). In contrast, vegetation decreases in Syria and Iraq, resulting in a larger vegetation factor and more dust emissions. However, similar to Australia, considering the strong variability, the trend is not very distinct because the highest vegetation factor in Iraq and Syria occurred in 2008 in the middle of the period of available data, whereas it decreased again in recent years.

2.3 Clay fraction

The efficiency of the sandblasting process is very sensitive to the clay fraction of the surface soil. Both very small and very large clay fractions are assumed to suppress the sandblasting efficiency. Our parametrisation of this dependency is discussed in section 3. Replacing the 1° clay fraction map of Scholes and Brown de Colstoun (2011), here we employ higher resolved clay fraction data from the *Global Soil Dataset for use in Earth System Models* (GSDE) (Shangguan et al., 2014), aggregated from 30" to 0.1°. The GSDE provides the clay fraction of the topmost 4.5 cm soil layer, which is most relevant for sandblasting rather than the clay fraction of the topmost 30 cm in the data of Scholes and Brown de Colstoun (2011). The two datasets are compared in Fig. S1 in the supplement.

3 Modifications to the emission scheme

Sandblasting efficiency: The sandblasting efficiency used by Astitha et al. (2012), based on the studies of Marticorena and Bergametti (1995) and Tegen (2002), increases exponentially with a clay fraction up to 20 %, beyond which the sandblasting is negligible, see Fig. 3. The resulting threshold is problematic in regions where the clay fraction is in the range of this discontinuity, for example in Iraq and Syria: small variations in the clay fraction can drastically alter the sandblasting efficiency between its maximum and essentially zero. Considering that both the clay fraction data and the sandblasting efficiency measurements are associated with uncertainty, we propose to apply a Gaussian filter. Figure 3 shows the efficiency after applying a filter with an interquartile range of 5 %, which is used in the validation simulation discussed below. The filter width could be optimised systematically, but in our experience results are robust by smoothing the distinct peak at 20 % clay fraction. Combining the filtered sandblasting efficiency with the updated clay fraction data (section 2.3) yields the global map presented in Fig. 4.

Soil moisture term: The original emission scheme of Astitha et al. (2012) applies a soil moisture dependent correction factor to the threshold friction velocity which increases the threshold and thus reduces dust emissions from wet soils. This correction factor has not been active in MESSy versions up to 2.52 and ~~since~~ the higher AOD over the Middle East obtained without the factor generally ~~more closely~~ resembles the satellite observations ~~, it is not used in the present study.~~ more closely, its impact when evaluated using soil moisture values from the current EMAC bucket model is rather small (see Fig. S2 in the supplement). Therefore, it remains inactive for the present study, consistent with previous studies (Abdelkader et al., 2015, 2016; Metzger et al., 2016; Al Nevertheless, the monthly vegetation data described above accounts for secondary effects of soil moisture variations via the vegetation factor. However, since the soil moisture is known to be a relevant parameter (Gherboudj et al., 2015) and, e.g., strongly correlates with the AOD over the Middle East (Klingmüller et al., 2016) ~~,~~ suggesting a direct link between surface drying and increasing dust emissions, we consider a detailed parametrisation of the soil moisture effect to be essential to capture the observed trends in future simulations. This will require a comprehensive soil model providing accurate moisture values for the topmost surface layer which has yet to be implemented in EMAC.

Surface friction velocity limit: The relation of the horizontal dust particle flux H and the surface friction velocity u_* is parametrised as a polynomial of degree 3,

$$H \propto (u_* + u_{*t})^2 (u_* - u_{*t}), \begin{cases} (u_* + u_{*\mathrm{t}})^2 (u_* - u_{*\mathrm{t}}) & u_* > u_{*\mathrm{t}} \\ 0 \end{cases} \tag{2}$$

where ~~u_{*t}~~ $u_{*\mathrm{t}}$ is the threshold friction-velocity. Therefore, high surface friction velocities occurring in mountainous regions can produce spuriously strong dust outbreaks where emissions are not limited by the updated landcover mask, vegetation factor or sandblasting efficiency, e.g. in Iran. To avoid this, we limit the ~~threshold~~ friction velocity in the above equation to a maximum value of 0.4 m / s. ~~The~~ Figure S3 in the supplement exemplifies the effect of using larger or smaller limits. The precise limit might be further adjusted but the given value yields good results as shown in Sect. 5.

Topography factor: In the original scheme, the accumulation of sediments in valleys and depressions is not considered explicitly and is only to some extent reflected implicitly by other input data such as the clay fraction. As shown by the reference simulation presented in Sect. 5, this can result in an underestimation of dust emissions from areas like the Tigris-Euphrates Basin. We therefore include a topography factor using the topographic source function proposed by Ginoux et al. (2001),

$$S_{\mathrm{topo}} = \left(\frac{z_{\mathrm{max}} - z}{z_{\mathrm{max}} - z_{\mathrm{min}}} \right)^5, \tag{3}$$

where z is the median elevation in a circle with $1°$ diameter and z_{min} (z_{max}) the minimum (maximum) elevation in the surrounding circle with $10°$ diameter. (Ginoux et al. (2001) use $1°$ pixels and the extreme values in the surrounding $10° \times 10°$ square). The Global Multi-resolution Terrain Elevation Data 2010 (GMTED2010) (Danielson and Gesch, 2011; GMTED2010, 2010) is used as topography data base. Figure 5 depicts a global map of the resulting topography factor. As the topography factor takes values between 0 and 1 and usually is smaller than 1, a normalisation factor $N \geq 1$ has to be multiplied to ~~conserve~~ avoid suppression of the global emissions. ~~Based on~~ In a one-month test simulation we ~~use~~ obtain a ratio between the global emissions without and including the factor S_{topo} of 5.3. Consequently, the full topography term we use is NS_{topo} where $N = 5.3$.

Mode mapping: The emission scheme considers emissions into three log-normal modes, adapting the parameters of the "background" modes of d'Almeida (1987) listed in table 2. Originally, these log-normal modes have been mapped to eight transport bins as used by Pérez et al. (2006), before being distributed to the accumulation and coarse mode of the EMAC aerosol submodel GMXE. We simplify this procedure by directly mapping the three emission modes to the two relevant

GMXE modes. The mass fraction M assigned to each GMXE mode is

$$M = \sum_{i=1}^{3} \frac{1}{2} \left(\mathrm{erf}\left(\frac{\ln(d_{\max}/\tilde{d}_i)}{\sqrt{2}\ln\sigma_{g,i}}\right) - \mathrm{erf}\left(\frac{\ln(d_{\min}/\tilde{d}_i)}{\sqrt{2}\ln\sigma_{g,i}}\right) \right), \tag{4}$$

where the sum encompasses over the three emission modes, $\tilde{d}_i$ and $\sigma_{g,i}$ are the mass median diameter and geometric standard deviation of each emission mode, and $d_{\min}$ and $d_{\max}$ are the threshold diameters of the GMXE mode. In practice, the modification is equivalent to a change of the threshold diameter between accumulation and coarse mode, which is now consistent with the GMXE parameters. Moreover, the algorithm generalises seamlessly when including additional GMXE modes such as a giant aerosol mode ($> 10\mu\mathrm{m}$).

Scaling factor: For the dimensionless empirical constant c by which the horizontal particle flux is scaled, Astitha et al. (2012) use the value $c = 1$, consistent with Darmenova et al. (2009). Since the dust emissions, especially in the Middled East, tend to underestimate the observations, we increase the value to $c = 1.5$, which is bounded by the original value and $c = 2.61$ used by White (1979) and Marticorena and Bergametti (1995). When switching to different model resolutions, the scaling factor can be used to balance potential resolution dependencies of the emission scheme. As will be discussed in section 5, with this value we obtain the same total amount of globally emitted dust as with the original emission scheme by Astitha et al. (2012). It should be stressed that the scaling factor is the central empirical tuning parameter of the emission scheme and might be improved by systematic optimisation, but our focus is on the spatiotemporal emission pattern which is largely unaffected by the overall scaling.

Chemical composition: In addition to the bulk dust flux output, we compute the Na^{+}, K^{+}, Ca^{++} and Mg^{++} fractions of the emitted dust, since mineral cations are important for the gas-aerosol partitioning (Metzger et al., 2006). For this purpose we have generated maps of the desert soil composition (Fig. 6) based on the fractions reported by Karydis et al. (2016) and geographical data from the Natural Earth dataset (Natural Earth, 2016). The chemical composition does not affect the amount of dust emitted, but the chemical ageing of airborne dust particles simulated by the GMXE submodel can affect the atmospheric residence time (Abdelkader et al., 2015) and the optical properties (Klingmüller et al., 2014).

4 Effects of the individual modifications

To compare the effects of the individual modifications we study the term $a\, f_{\mathrm{landcover}}\, f_{\mathrm{veg}}\, N\, S_{\mathrm{topo}}$ (cf. Eq. (A2) in the appendix), the product of the clay fraction dependent sandblasting efficiency a, the barren land fraction $f_{\mathrm{landcover}}$, the vegetation factor f_{veg} and the normalised topography factor $N\, S_{\mathrm{topo}}$. It is proportional to the dust emission flux (given that the threshold surface friction velocity is exceeded) and reflects the effects of the modifications independently of the precise wind conditions. Figure 7 compares the term during July 2011 for the reference and validation simulations, and variations of the validation setup selectively using either the landcover, sandblasting efficiency, clay fraction or vegetation data from the reference scheme, or omitting the topography factor. The update of the landcover data, the inclusion of the topography factor and the modification to the sandblasting efficiency distinctively affect the dust emissions, whereas the update of clay fraction and vegetation data have a more subtle effect (see also Fig. S4 in the supplement). The latter implies that the effect of the seasonal cycle in the vegetation data is not clearly visible in this representation, justifying to study only July in Fig. 7. The landcover update clearly expands the source regions of the dust belt. The topography factor redistributes the emissions enhancing emissions from basins (e.g., the Tigris-Euphrates Basin) while reducing emissions from mountenous areas. Omitting the topography factor the revised scheme produces a much more homogeneous distribution. The revised sandblasting efficiency avoids pixels with very strong or very little emissions in regions with a clay fraction of around 20 %. In such regions, reverting to the original sandblasting efficiency yields peaks of extremely high emission factors, defining the upper limit of the colour scale in Fig. 7. This is especially the case in regions where the original scheme suppressed emissions based on the landcover classification, therefore the revised sandblasting efficiency is mandatory when using the updated landcover data. Most importantly, to the benefit of future high resolution simulations with truncations of T255 or higher ($<$ 50km grid spacing), the updates considerably increase the resolution of the emission factor as illustrated by the column on the right hand side of Fig. 7.

5 Validation

We use EMAC in the combination ECHAM 5.3.02 and MESSy 2.52 at horizontal resolution T106 with 31 vertical levels. The Gaussian T106 grid has a grid spacing of $1.125°$ along the latitudes and about $1.121°$ along the longitudes. At the equator, this corresponds to virtually quadratical cells with around 125 km edge length. The following MESSy submodels have been enabled: AEROPT, AIRSEA, CLOUD, CLOUDOPT, CONVECT, CVTRANS, DDEP, GMXE, JVAL, LNOX, MECCA, OFFEMIS, ONEMIS, ORBIT, ORACLE, PTRAC, RAD, SCAV, SEDI, SURFACE, TNUDGE, TROPOP. Descriptions of each submodel and further references can be found online in the MESSy submodel list (MESSy 2017). The dust emission scheme is evaluated by the online emission submodel ONEMIS, the aerosol microphysical processes are simulated by the Global Model aerosol eXtEnsion (GMXE) submodel (Pringle et al., 2010a, b). Within GMXE two gas-aerosol partitioning schemes are available, ISOROPIA ISORROPIA II (Fountoukis and Nenes, 2007) and EQSAM4clim (Metzger et al., 2016), here we employ the former. The prognostic radiative-transfer calculation uses the Tanre aerosol climatology for extinction, single scattering albedo and asymmetry factor (Tanre et al., 1984), and the model dynamics above the boundary layer are nudged to meteorological analyses of the European Centre for Medium-Range Weather Forecasts (ECMWF). The CMIP5 (Coupled Model Intercomparison Project), GFEDv3.1 (Global Fire Emissions Database) and AeroCom (Aerosol Comparisons between Observations and Models) databases provide anthropogenic, biomass burning and sea salt emissions, respectively.

Two simulations are considered: a reference simulation using the original emission scheme and a validation simulation using the updated input data presented in Sect. 2 and the modifications presented in Sect. 3. The different input datasets are summarised in table 1. The chemical composition of the emitted particles is considered in both simulations. As validation time period we selected the year 2011. 2011 to represent a recent period well past the time period on which the former input data was based on. The simulations are initialised at 1 July 2010 from the output of a lower resolving T42 simulation starting in 1998. After this initialisation, six months simulated with the final T106 resolution serve as additional spin-up period.

To quantify the (dis)agreement of model results and observations we use the skill score S defined by Taylor (2001),

$$S = \frac{4(1+r)^4}{(\sigma_1/\sigma_2 + \sigma_2/\sigma_1)^2(1+r_0)^4}, \tag{5}$$

where r is the correlation coefficient and σ_1 and σ_2 are the standard deviations of modelled and observed values. As maximum attainable correlation coefficient we simply use $r_0 = 1$ since we are predominantly interested in the relative changes of the skill score resulting from our modifications to the dust emission scheme. A more accurate estimate $r_0 < 1$ would result in higher skill scores.

Both simulations obtain the same global mineral dust emission of 1.3 Gt in 2011 (Table 3), which is well in the range of values reported by Huneeus et al. (2011) and close to their median of 1.1 Gt per year. Aligning the threshold between accumulation and coarse mode with GMXE as described in section 3 for the parameters shown in Table 2 results in more accumulation mode emissions in the validation simulation (0.15 Gt / year) than in the reference simulation (0.052 Gt / year), thus higher 550 nm AOD values are expected in the former.

5.1 AERONET

For the comparison with Aerosol Robotic Network (AERONET) (Holben et al., 1998; AERONET) AOD observations, we select regions based on the relevance of the regional dust emissions and the abundance of AERONET stations. We focus on the ~~six~~ seven regions of interest depicted in Fig. 8 encompassing the Middle East (~~region A), Africa (B),~~ *ME*), north-west Africa (*N. Afr.*), Africa, Central and East Asia (~~C~~*Asia*), the south-west of the United States of America (~~D~~*N. Amer.*), the Southern Cone ~~(E~~in South America (*S. A.*) and Australia (~~F~~*Austral.*). All stations with observations during at least 120 days distributed over at least 9 months of 2011 are considered.

We compare daily averages of modelled and observed aerosol optical depth (AOD) at 550 nm, where the AERONET AOD at this wavelength is obtained from level 2 data by interpolation using the Ångström exponent. For each station we use the model values from the grid cell covering the station coordinates. The skill score S is shown in Fig. 9. For most stations, the validation simulation achieves higher skill scores than the reference simulation (time series plots for the stations with the highest increase are shown in Fig. S5 in the supplement), similar skill scores are obtained for the Australian stations. Only over four stations in north-west Africa the validation simulations produces noticeably lower skill scores than the reference run. However, the skill scores for these stations remain among the highest globally. Moreover, the two stations with the strongest skill score degradation are located very close to each other on the island Tenerife, in Santa Cruz de Tenerife and at the Izana Atmospheric Observatory on Mount Teide. In contrast, the validation skill score for a third station on Tenerife, in La Laguna, is marginally larger than the corresponding reference skill score.

Studying the AOD time series for these three stations (Fig. 10 top), reveals that over Santa Cruz de Tenerife the model slightly overestimates the observations and the even higher AOD levels in the validation simulation result in the lower skill score. On the other hand, dust events observed by AERONET in January and December are reproduced by the validation simulation, but not by the reference simulation. The Izana station on Mount Teide is special: located at 2391 m altitude, it shares the same model grid cell with the La Laguna station at 568 m altitude, Fig. 10 (bottom), but naturally the observed AOD is much lower. Obviously, the station site is not well represented by the model grid cell, which predominantly covers open sea and has a surface altitude of 63 m. These considerations put the regression of the skill score over the Canaries into perspective and suggest that some overestimation of the AOD over north-west Africa in the validation simulation is an acceptable trade-off in view of the skill score increase elsewhere. This conclusion is further supported by the comparison with MODIS observations in the following section.

5.2 MODIS

To verify the global aerosol distribution, we validate the model AOD against observations from the Terra satellite provided by the Moderate-resolution Imaging Spectroradiometer (MODIS) data collection 6 (Hubanks et al., 2015; Levy et al., 2013; MODIS MOD08 M3). We use the merged 550 nm AOD combining retrievals from the Deep Blue and Dark Target algorithms (Sayer et al., 2014).

Figure 11 compares the 2011 annual mean AOD from the two simulations and MODIS. The AOD levels over the Sahara and the Middle East produced by the validation simulation agree well with the observed levels, whereas they are underestimated by the reference simulation. Features of the MODIS distribution found in the validation but not in the reference result are regionally high AOD values over the Middle East along the Gulf and extending over Iraq and Syria, and the absence of a local maximum over Argentina. The latter is even more evident at higher wavelengths considered in the following section. Over west Africa, the high AOD levels in the validation simulation extend slightly further north than observed by MODIS. This is consistent with the overestimation of AERONET observations in that region discussed above, but does not considerably compromise the globally improved agreement with MODIS.

The improved agreement of the AOD distribution obtained by the validation simulation can be quantified by correlating the pixel values of the equivalent maps shown in Fig. 11. The revised dust emissions enhance the spatial correlation of the AOD pattern from 0.79 to 0.81 and the skill score from 0.58 to 0.67.

Fig. 12 zooms into the Middle East (Region A) to illustrate the annual variability of the 550 nm AOD by showing seasonal means. Especially in Spring and Summer, the enhanced AOD levels along the Tigris-Euphrates Basin and the Gulf are clearly visible in the validation result, consistent with the MODIS observations, while not being represented in the reference results. During summer, the validation simulation produces higher AOD levels also over Arabian and Red Sea, which are closer to the extremely high levels reported by MODIS and Brindley et al. (2015). Surprisingly, the MODIS AOD over Iran is close to zero throughout the year, but substantial levels are obtained during spring and summer by both simulations, with higher levels in the validation simulation than in the reference simulation. The strong seasonal cycle over the Middle East observed by MODIS is reproduced by both simulations, but with its higher spring and summer AOD levels, the validation simulation yields a higher amplitude in better agreement with MODIS. To underscore the improvement achieved by the revised emissions, we quantify the spatial agreement of the seasonal AOD over the Arabian Peninsula including Syria, Iraq and Jordan using the correlation coefficient and the skill score (see Fig. S6 in the supplement). Both measures show a significant increase throughout the year, especially during winter (the correlation coefficient from 0.18 to 0.54, the skill score from 0.068 to 0.24) and summer (the correlation coefficient from 0.46 to 0.75, the skill score from 0.22 to 0.55). The global seasonal AOD distribution is shown in Figs. S8 to S11 in the supplement.

5.3 IASI

To focus the evaluation more tightly on dust, we utilise data from the *Infrared Atmospheric Sounding Interferometer* (IASI) (Clerbaux et al., 2009; Hilton et al., 2012) provided by the Aerosol-CCI (Climate Change Initiative) project (Popp et al., 2016; IASI) of the *European Space Agency* (ESA). We use version 7 of the level 3 monthly dust AOD (DAOD) at 10 μm prepared at the Université Libre de Bruxelles (IASI_ULB.v7). The corresponding annual average DAOD map for 2011 is shown in the middle panel of Fig. 13.

To compare with the IASI DAOD, we filter the daily 10 μm EMAC AOD considering only dust dominated values as DAOD, setting the DAOD to zero if sea salt dominates instead. The contribution of both components is quantified by weighting the AOD of each mode with the volume fraction of the component. The diagnostic output of optical properties at wavelengths up to 10 μm has not been utilised previously in EMAC though proves very valuable to compare with remotely sensed optical properties of coarse particles such as aeolian dust. The annual average for 2011 from validation and reference simulation are shown in the top and bottom panel of Fig. 13. In several aspects the DAOD distribution obtained by the validation simulation resembles the IASI observations more closely. In the Middle East, the region of high dust loads distinctly extends north-westwards into the Fertile Crescent, whereas comparably low dust loads are found over the western half of the Arabian Peninsula. The DAOD is more pronounced over Pakistan, and similarly over Djibouti and the adjacent regions south-west of the Red Sea. The regional maximum over Chad is less distinct than in the reference simulation. Over the Southern Andes, the maximum obtained by the reference simulation, though not detected by IASI, is not reproduced by the validation simulation, which is distinctly more realistic.

The correlation coefficient of the validation result and IASI is ~~0.87~~ 0.89 compared to 0.79 for the reference simulation, the corresponding skill score is enhanced by our modifications from ~~0.62 to 0.76~~0.64 to 0.78.

The annual variability of the 10 μm DAOD over the Middle East (Region A) is compared in Fig. 14. As for the AOD, in spring and summer, the high DAOD values along the Tigris-Euphrates Basin are clearly visible in the validation result, consistent with the IASI observations, while not being represented in the reference result. During summer, the DAOD pattern obtained by the validation simulation at the southern Red Sea resembles the pattern observed by IASI, even though the observed regional maximum is more pronounced. Also the DAOD at the Iranian and Pakistani Arabian Sea coast produced by the validation simulation agrees more closely with the IASI result. The reference simulation does not produce dust over the Caspian Sea and to its south, whereas IASI obtains significant DAOD values in spring and summer. These are reproduced by the validation simulation but seem to be slightly overestimated during summer. The strong seasonal cycle observed by IASI is realistically reproduced by both simulations. We quantify the apparent improvement achieved by the revised emissions by assessing the spatial agreement of the seasonal AOD over the Arabian Peninsula (including Syria, Iraq and Jordan) using the correlation coefficient and the skill score (see Fig. S7 in the supplement). The increase obtained for both measures throughout the year is significant for most seasons, especially during autumn for which the correlation coefficient increases from 0.30 to 0.62, the skill score from 0.14 to 0.39. The global seasonal DAOD distribution is shown in Figs. S12 to S15 in the supplement.

5.4 Dust concentration and deposition

We use dust concentration and deposition data from the AEROCOM dust benchmark dataset (Huneeus et al., 2011) to evaluate the corresponding results of our simulations. Concentration climatologies from 25 sites with in total 292 monthly values and the annual dust deposition rates from 84 sites are considered for our evaluation (see Fig. S16 in the supplement).

The deposition obtained by the validation simulation agrees significantly better with the observations than the reference result (Fig. 15), with a correlation coefficient of 0.89 compared to 0.80 and a skill score of 0.78 compared to 0.64. Regarding the concentration, the two simulations show no significant difference in performance.

At sites with low dust concentrations both simulations underestimate the observed concentrations which could be either due to an underestimation of dust transport in the model or due to local non-desert dust sources not represented in the dust emission schemes.

6 Conclusions

We have prepared new input data for use with the EMAC dust emission scheme developed by Astitha et al. (2012), and proposed changes and extensions. With a geographic representation of at least $0.1°$ for all input parameters, the updated input data has a significantly higher spatial resolution than the data used thus far. Therefore, the new data will be important for use in planned high resolution simulations with truncations of T255 or higher ($< 50\mathrm{km}$). The land cover and vegetation in the updated data is time dependent, so that the effect of long-term trends and variability of these quantities on the dust emissions are taken into account. In addition to the input parameters used by the original implementation by Astitha et al. (2012), we take the topography into account, which enhances the emissions from basins and valleys such as the Tigris-Euphrates region and the Afar Triangle, in better agreement with observations. Moreover, we have produced soil composition maps to differentiate the chemical composition of dust particles from different deserts that affects the coating of mineral dust by hygroscopic salts during atmospheric ageing.

The updated landcover classification, the inclusion of the topography factor and the modification of the sandblasting efficiency function have a considerable impact on the global and regional distribution of dust emissions. By comparison, the effect of the clay fraction and vegetation data updates is less distinct.

The updated input data in combination with the adjustments to the emission scheme improve the modelled AOD and DAOD, as demonstrated by the comparison with AERONET, MODIS and IASI observations. For this validation, we have evaluated the EMAC DAOD at wavelengths up to $10\ \mu\mathrm{m}$ for the first time, which allows testing of the model with a focus on dust, i.e. based on IASI DAOD.

Also the comparison with dust deposition observations shows improved agreement when using the updated emissions. This is less clear for the comparison with dust concentration data, where original and updated emission scheme do not show a significant performance difference.

While the updates clearly improve the global distribution of aeolian dust, the total amount of globally emitted dust remains unchanged and consistent with literature values.

Subject to the future availability of suitable soil models in EMAC providing soil moisture values for a thin surface soil layer, the activation of the explicit soil moisture dependency of the threshold surface friction velocity might further improve the agreement with observed trends and variability.

Code and data availability

The Modular Earth Submodel System (MESSy) is continuously further developed and applied by a consortium of institutions. The usage of MESSy and access to the source code is licenced to all affiliates of institutions which are members of the MESSy Consortium. Institutions can become a member of the MESSy Consortium by signing the MESSy Memorandum of Understanding. More information can be found on the MESSy Consortium Website (http://www.messy-interface.org). The input data files and all modifications to the EMAC source code presented in this article are available on request until they become part of the official MESSy code.

Acknowledgements. The research reported in this publication has received funding from the King Abdullah University of Science and Technology (KAUST) CRG3 grant URF/1/2180-01 *Combined Radiative and Air Quality Effects of Anthropogenic Air Pollution and Dust over the Arabian Peninsula*. S. Metzger receives funding from the European Commission through the H2020-EINFRA-2015-1 project “Energy oriented Centre of Excellence for computer applications (EoCoE)”, Proposal number: 676629.

Appendix A: Emission equation

In the DU_Astitha1 emission scheme (Astitha et al., 2012), the threshold surface friction velocity u_{*t} is obtained by the equation

$$
\begin{aligned}
u_{*t} =& 0.129 \sqrt{\frac{D_\mathrm{p}}{\rho_\mathrm{air}} \left(\rho_\mathrm{p} g + \frac{0.006 \mathrm{g} \sqrt{\mathrm{cm}}/\mathrm{s}^2}{D_\mathrm{p}^{5/2}} \right)} \\
& \times \begin{cases} \frac{1}{\sqrt{1.928 B^{0.092} - 1}} & B < 10 \\ (1 - 0.0858 e^{-0.0617(B-10)}) & B \geq 10 \end{cases} \\
& \times \left(1 - \frac{\ln \frac{z_\mathrm{o}}{z_\mathrm{os}}}{\ln(0.35 \left(\frac{10\mathrm{cm}}{z_\mathrm{os}} \right)^{0.8})} \right)^{-1} \\
& \times \sqrt{1 + 1.21 \max(0, \left(w - (0.0014 \phi_\mathrm{clay}^2 + 0.17 \phi_\mathrm{clay}) \right))^{0.68}},
\end{aligned}
\quad \text{(A1)}
$$

where

$D_\mathrm{p} = 60\ \mu m$	saltation particle diameter
ρ_air	air density
$\rho_\mathrm{p} = 2.65\ \mathrm{g/cm^3}$	particle density
$g = 9.80665\ \mathrm{m/s^2}$	gravitational acceleration
$B = \frac{u_{*t} D_\mathrm{p}}{v}$	friction Reynolds number,
	initially $B = 1331 (D_\mathrm{p}/\mathrm{cm})^{1.56} + 0.38$
$v = 0.157 \cdot 10^{-4}\ \mathrm{m^2/s}$	kinematic viscosity of air
$z_\mathrm{o} = 0.01\ \mathrm{cm}$	surface roughness length
$z_\mathrm{os} = 0.00333\ \mathrm{cm}$	local roughness length of the uncovered surface
w	gravimetric soil moisture in %
ϕ_clay	clay fraction in %

The last, soil moisture term in Eq. (A1) is omitted in the present study. If the surface friction velocity u_* exceeds the threshold u_{*t}, the resulting emission flux is computed according to the equation

$$
j_{\mathrm{emis}\mathrm{emis},i} = \frac{c \rho_\mathrm{air}}{g} (u_* + u_{*t})^2 (u_* - u_{*t})\ 10^{-4}\ a\ f_\mathrm{landcover}\ f_\mathrm{veg} M_i, \quad \text{(A2)}
$$

where

i	mode index
$c = 1$	empirical constant (in this study $c = 1.5$)
~~$g = 9.80665\ \mathrm{m/s^2}$ gravitational acceleration~~ u_*	surface friction velocity
$f_{\mathrm{landcover}}$	barren land fraction
$f_{\mathrm{veg}} = 1 - \frac{\min(\mathrm{LAI}, 0.35)}{0.35}$	vegetation factor
a	sandblasting efficiency
M_i	mass fraction emitted into mode i

In the present study we multiply the right-hand side of Eq. (A2) with the topography factor $S_{\mathrm{topo}} = ((z_{\max} - z)/(z_{\max} - z_{\min}))^5$ defined in Eq. (3) and the corresponding normalisation factor $N = 5.3$. In addition, the surface friction velocity u_* is limited to a maximal value of $0.4\ \mathrm{m/s}$, i.e., u_* in Eq. (A2) is replaced by $\min(u_*, 0.4\ \mathrm{m/s})$.

References

Abdelkader, M., Metzger, S., Mamouri, R. E., Astitha, M., Barrie, L., Levin, Z., and Lelieveld, J.: Dust–air pollution dynamics over the eastern Mediterranean, Atmospheric Chemistry and Physics, 15, 9173–9189, doi:10.5194/acp-15-9173-2015, http://www.atmos-chem-phys.net/15/9173/2015/, 2015.

Abdelkader, M., Metzger, S., Steil, B., Klingmüller, K., Tost, H., Pozzer, A., Stenchikov, G., Barrie, L., and Lelieveld, J.: Chemical aging of atmospheric mineral dust during transatlantic transport, Atmospheric Chemistry and Physics Discussions, 2016, 1–36, doi:10.5194/acp-2016-470, http://www.atmos-chem-phys-discuss.net/acp-2016-470/, 2016.

AERONET: http://aeronet.gsfc.nasa.gov, visited 31 Aug 2016.

Albani, S., Mahowald, N. M., Perry, A. T., Scanza, R. A., Zender, C. S., Heavens, N. G., Maggi, V., Kok, J. F., and Otto-Bliesner, B. L.: Improved dust representation in the Community Atmosphere Model, Journal of Advances in Modeling Earth Systems, 6, 541–570, doi:10.1002/2013MS000279, 2014.

Allen, C. J. T., Washington, R., and Engelstaedter, S.: Dust emission and transport mechanisms in the central Sahara: Fennec ground-based observations from Bordj Badji Mokhtar, June 2011, Journal of Geophysical Research: Atmospheres, 118, 6212–6232, doi:10.1002/jgrd.50534, 2013.

Allen, C. J. T., Washington, R., and Saci, A.: Dust detection from ground-based observations in the summer global dust maximum: Results from Fennec 2011 and 2012 and implications for modeling and field observations, Journal of Geophysical Research: Atmospheres, 120, 897–916, doi:10.1002/2014JD022655, 2015.

Anisimov, A., Tao, W., Stenchikov, G., Kalenderski, S., Jish Prakash, P., Yang, Z.-L., and Shi, M.: Quantifying local-scale dust emission from the Arabian Red Sea coastal plain, Atmospheric Chemistry and Physics, 17, 993–1015, doi:10.5194/acp-17-993-2017, 2017.

Astitha, M., Lelieveld, J., Abdel Kader, M., Pozzer, A., and de Meij, A.: Parameterization of dust emissions in the global atmospheric chemistry-climate model EMAC: impact of nudging and soil properties, Atmospheric Chemistry and Physics, 12, 11 057–11 083, doi:10.5194/acp-12-11057-2012, 2012.

Balkanski, Y., Schulz, M., Claquin, T., Moulin, C., and Ginoux, P.: Global Emissions of Mineral Aerosol: Formulation and Validation using Satellite Imagery, pp. 239–267, Springer Netherlands, Dordrecht, doi:10.1007/978-1-4020-2167-1_6, http://dx.doi.org/10.1007/978-1-4020-2167-1_6, 2004.

Bonan, G. B., Levis, S., Kergoat, L., and Oleson, K. W.: Landscapes as patches of plant functional types: An integrating concept for climate and ecosystem models, Global Biogeochemical Cycles, 16, 5–1–5–23, doi:10.1029/2000GB001360, http://dx.doi.org/10.1029/2000GB001360, 2002.

Brindley, H., Osipov, S., Bantges, R., Smirnov, A., Banks, J., Levy, R., Jish Prakash, P., and Stenchikov, G.: An assessment of the quality of aerosol retrievals over the Red Sea and evaluation of the climatological cloud-free dust direct radiative effect in the region, Journal of Geophysical Research: Atmospheres, 120, 10, doi:10.1002/2015JD023282, 2015.

Clerbaux, C., Boynard, A., Clarisse, L., George, M., Hadji-Lazaro, J., Herbin, H., Hurtmans, D., Pommier, M., Razavi, A., Turquety, S., Wespes, C., and Coheur, P.-F.: Monitoring of atmospheric composition using the thermal infrared IASI/MetOp sounder, Atmospheric Chemistry and Physics, 9, 6041–6054, doi:10.5194/acp-9-6041-2009, 2009.

d'Almeida, G. A.: On the variability of desert aerosol radiative characteristics, Journal of Geophysical Research, 92, 3017, doi:10.1029/JD092iD03p03017, 1987.

Danielson, J. J. and Gesch, D. B.: Global Multi-resolution Terrain Elevation Data 2010 (GMTED2010), U.S. Geological Survey Open-File Report, http://pubs.usgs.gov/of/2011/1073/pdf/of2011-1073.pdf, 2011.

Darmenova, K., Sokolik, I. N., Shao, Y., Marticorena, B., and Bergametti, G.: Development of a physically based dust emission module within the Weather Research and Forecasting (WRF) model: Assessment of dust emission parameterizations and input parameters for source regions in Central and East Asia, Journal of Geophysical Research: Atmospheres, 114, D14 201, doi:10.1029/2008JD011236, 2009.

Dong, B. and Sutton, R.: Dominant role of greenhouse-gas forcing in the recovery of Sahel rainfall, Nature Climate Change, 5, 757–760, doi:10.1038/nclimate2664, 2015.

Fountoukis, C. and Nenes, A.: ISORROPIA II: a computationally efficient thermodynamic equilibrium model for K^+-Ca^{2+}-Mg^{2+}-${NH_4}^+$-Na^+-${SO_4}^{2-}$-${NO_3}^-$-Cl^--H_2O aerosols, Atmospheric Chemistry and Physics, 7, 4639–4659, doi:10.5194/acp-7-4639-2007, http://www.atmos-chem-phys.net/7/4639/2007/, 2007.

Gherboudj, I., Beegum, S. N., Marticorena, B., and Ghedira, H.: Dust emission parameterization scheme over the MENA region: Sensitivity analysis to soil moisture and soil texture, Journal of Geophysical Research: Atmospheres, 120, 10, doi:10.1002/2015JD023338, 2015.

Giannadaki, D., Pozzer, A., and Lelieveld, J.: Modeled global effects of airborne desert dust on air quality and premature mortality, Atmospheric Chemistry and Physics, 14, 957–968, doi:10.5194/acp-14-957-2014, http://www.atmos-chem-phys.net/14/957/2014/, 2014.

Ginoux, P., Chin, M., Tegen, I., Prospero, J. M., Holben, B., Dubovik, O., and Lin, S.-J.: Sources and distributions of dust aerosols simulated with the GOCART model, Journal of Geophysical Research: Atmospheres, 106, 20 255–20 273, doi:10.1029/2000JD000053, 2001.

Gläser, G., Kerkweg, A., and Wernli, H.: The Mineral Dust Cycle in EMAC 2.40: sensitivity to the spectral resolution and the dust emission scheme, Atmospheric Chemistry and Physics, 12, 1611–1627, doi:10.5194/acp-12-1611-2012, http://www.atmos-chem-phys.net/12/1611/2012/, 2012.

GMTED2010: https://lta.cr.usgs.gov/GMTED2010, visited 24 Aug 2016, 2010.

Hilton, F., Armante, R., August, T., Barnet, C., Bouchard, A., Camy-Peyret, C., Capelle, V., Clarisse, L., Clerbaux, C., Coheur, P.-F., Collard, A., Crevoisier, C., Dufour, G., Edwards, D., Faijan, F., Fourrié, N., Gambacorta, A., Goldberg, M., Guidard, V., Hurtmans, D., Illingworth, S., Jacquinet-Husson, N., Kerzenmacher, T., Klaes, D., Lavanant, L., Masiello, G., Matricardi, M., McNally, A., Newman, S., Pavelin, E., Payan, S., Péquignot, E., Peyridieu, S., Phulpin, T., Remedios, J., Schlüssel, P., Serio, C., Strow, L., Stubenrauch, C., Taylor, J., Tobin, D., Wolf, W., and Zhou, D.: Hyperspectral Earth Observation from IASI: Five Years of Accomplishments, Bulletin of the American Meteorological Society, 93, 347–370, doi:10.1175/BAMS-D-11-00027.1, 2012.

Holben, B., Eck, T., Slutsker, I., Tanré, D., Buis, J., Setzer, A., Vermote, E., Reagan, J., Kaufman, Y., Nakajima, T., Lavenu, F., Jankowiak, I., and Smirnov, A.: AERONET—A Federated Instrument Network and Data Archive for Aerosol Characterization, Remote Sensing of Environment, 66, 1–16, doi:10.1016/S0034-4257(98)00031-5, 1998.

Hubanks, P., Platnick, S., King, M., and Ridgway, B.: MODIS Atmosphere L3 Gridded Product Algorithm Theoretical Basis Document (ATBD) & Users Guide, 2015.

Huneeus, N., Schulz, M., Balkanski, Y., Griesfeller, J., Prospero, J., Kinne, S., Bauer, S., Boucher, O., Chin, M., Dentener, F., Diehl, T., Easter, R., Fillmore, D., Ghan, S., Ginoux, P., Grini, A., Horowitz, L., Koch, D., Krol, M. C., Landing, W., Liu, X., Mahowald, N., Miller, R., Morcrette, J.-J., Myhre, G., Penner, J., Perlwitz, J., Stier, P., Takemura, T., and Zender, C. S.: Global dust model intercomparison in AeroCom phase I, Atmospheric Chemistry and Physics, 11, 7781–7816, doi:10.5194/acp-11-7781-2011, 2011.

IASI: http://www.esa-aerosol-cci.org/, visited 31 Aug 2016.

IPCC, ed.: Climate Change 2013 – The Physical Science Basis, Cambridge University Press, http://dx.doi.org/10.1017/CBO9781107415324, cambridge Books Online, 2014.

Jöckel, P., Sander, R., Kerkweg, A., Tost, H., and Lelieveld, J.: Technical Note: The Modular Earth Submodel System (MESSy) - a new approach towards Earth System Modeling, Atmospheric Chemistry and Physics, 5, 433–444, doi:10.5194/acp-5-433-2005, http://www.atmos-chem-phys.net/5/433/2005/, 2005.

Jöckel, P., Kerkweg, A., Pozzer, A., Sander, R., Tost, H., Riede, H., Baumgaertner, A., Gromov, S., and Kern, B.: Development cycle 2 of the Modular Earth Submodel System (MESSy2), Geoscientific Model Development, 3, 717–752, doi:10.5194/gmd-3-717-2010, http://www.geosci-model-dev.net/3/717/2010/, 2010.

Jones, S. L., Adams-Selin, R., Hunt, E. D., Creighton, G. A., and Cetola, J. D.: Update on modifications to WRF-CHEM GOCART for fine-scale dust forecasting at AFWA, AGU Fall Meeting Abstracts, 2012.

Karydis, V. A., Tsimpidi, A. P., Pozzer, A., Astitha, M., and Lelieveld, J.: Effects of mineral dust on global atmospheric nitrate concentrations, Atmospheric Chemistry and Physics, 16, 1491–1509, doi:10.5194/acp-16-1491-2016, 2016.

Kergoat, L., Moulin, S., Cayrol, P., and Dedieu, G.: Controlling vegetation growth models with satellite measurements, in: Advances in environmental and ecological modelling, edited by F., B. and A., W., pp. 73–89, Elsevier Publishers, 1999.

Klingmüller, K., Steil, B., Brühl, C., Tost, H., and Lelieveld, J.: Sensitivity of aerosol radiative effects to different mixing assumptions in the AEROPT 1.0 submodel of the EMAC atmospheric-chemistry–climate model, Geoscientific Model Development, 7, 2503–2516, doi:10.5194/gmd-7-2503-2014, 2014.

Klingmüller, K., Pozzer, A., Metzger, S., Stenchikov, G. L., and Lelieveld, J.: Aerosol optical depth trend over the Middle East, Atmospheric Chemistry and Physics, 16, 5063–5073, doi:10.5194/acp-16-5063-2016, http://www.atmos-chem-phys.net/16/5063/2016/, 2016.

Klose, M., Shao, Y., Li, X., Zhang, H., Ishizuka, M., Mikami, M., and Leys, J. F.: Further development of a parameterization for convective turbulent dust emission and evaluation based on field observations, Journal of Geophysical Research: Atmospheres, 119, 10, doi:10.1002/2014JD021688, 2014.

Kok, J. F., Mahowald, N. M., Fratini, G., Gillies, J. A., Ishizuka, M., Leys, J. F., Mikami, M., Park, M.-S., Park, S.-U., Van Pelt, R. S., and Zobeck, T. M.: An improved dust emission model - Part 1: Model description and comparison against measurements, Atmospheric Chemistry and Physics, 14, 13 023–13 041, doi:10.5194/acp-14-13023-2014, 2014.

Lamchin, M., Lee, J.-Y., Lee, W.-K., Lee, E. J., Kim, M., Lim, C.-H., Choi, H.-A., and Kim, S.-R.: Assessment of land cover change and desertification using remote sensing technology in a local region of Mongolia, Advances in Space Research, 57, 64–77, doi:10.1016/j.asr.2015.10.006, 2016.

Laurent, B., Marticorena, B., Bergametti, G., Léon, J. F., and Mahowald, N. M.: Modeling mineral dust emissions from the Sahara desert using new surface properties and soil database, Journal of Geophysical Research: Atmospheres, 113, n/a–n/a, doi:10.1029/2007JD009484, http://dx.doi.org/10.1029/2007JD009484, d14218, 2008.

Laurent, B., Tegen, I., Heinold, B., Schepanski, K., Weinzierl, B., and Esselborn, M.: A model study of Saharan dust emissions and distributions during the SAMUM-1 campaign, Journal of Geophysical Research: Atmospheres, 115, n/a–n/a, doi:10.1029/2009JD012995, http://dx.doi.org/10.1029/2009JD012995, d21210, 2010.

Levy, R. C., Mattoo, S., Munchak, L. A., Remer, L. A., Sayer, A. M., Patadia, F., and Hsu, N. C.: The Collection 6 MODIS aerosol products over land and ocean, Atmospheric Measurement Techniques, 6, 2989–3034, doi:10.5194/amt-6-2989-2013, 2013.

Mahowald, N., Kohfeld, K., Hansson, M., Balkanski, Y., Harrison, S. P., Prentice, I. C., Schulz, M., and Rodhe, H.: Dust sources and deposition during the last glacial maximum and current climate: A comparison of model results with paleodata from ice cores and marine sediments, Journal of Geophysical Research: Atmospheres, 104, 15 895–15 916, doi:10.1029/1999JD900084, http://dx.doi.org/10.1029/1999JD900084, 1999.

Marsham, J. H., Hobby, M., Allen, C. J. T., Banks, J. R., Bart, M., Brooks, B. J., Cavazos-Guerra, C., Engelstaedter, S., Gascoyne, M., Lima, A. R., Martins, J. V., McQuaid, J. B., O'Leary, A., Ouchene, B., Ouladichir, A., Parker, D. J., Saci, A., Salah-Ferroudj, M., Todd, M. C., and Washington, R.: Meteorology and dust in the central Sahara: Observations from Fennec supersite-1 during the June 2011 Intensive Observation Period, Journal of Geophysical Research: Atmospheres, 118, 4069–4089, doi:10.1002/jgrd.50211, 2013.

Marticorena, B. and Bergametti, G.: Modeling the atmospheric dust cycle: 1. Design of a soil-derived dust emission scheme, Journal of Geophysical Research, 100, 16 415, doi:10.1029/95JD00690, 1995.

Marticorena, B., Bergametti, G., Aumont, B., Callot, Y., N'Doumé, C., and Legrand, M.: Modeling the atmospheric dust cycle: 2. Simulation of Saharan dust sources, Journal of Geophysical Research: Atmospheres, 102, 4387–4404, doi:10.1029/96JD02964, http://dx.doi.org/10.1029/96JD02964, 1997.

MESSy 2017: MESSy submodel list, http://www.messy-interface.org/current/auto/messy_submodels.html, visited 2 Nov 2017.

Metzger, S., Mihalopoulos, N., and Lelieveld, J.: Importance of mineral cations and organics in gas-aerosol partitioning of reactive nitrogen compounds: case study based on MINOS results, Atmospheric Chemistry and Physics, 6, 2549–2567, doi:10.5194/acp-6-2549-2006, 2006.

Metzger, S., Steil, B., Abdelkader, M., Klingmüller, K., Xu, L., Penner, J. E., Fountoukis, C., Nenes, A., and Lelieveld, J.: Aerosol water parameterisation: a single parameter framework, Atmospheric Chemistry and Physics, 16, 7213–7237, doi:10.5194/acp-16-7213-2016, http://www.atmos-chem-phys.net/16/7213/2016/, 2016.

MODIS MCD12C1: ftp://ladsweb.nascom.nasa.gov/allData/51/MCD12C1/, visited 9 Jun 2016.

MODIS MOD08 M3: ftp://ladsweb.nascom.nasa.gov/allData/6/MOD08_M3/, visited 24 May 2017.

Natural Earth: http://www.naturalearthdata.com, visited 16 Nov 2016, 2016.

Olson, J.: World Ecosystems (WE1.4): Digital raster data on a 10 minute geographic 1080 x 2160 grid, in: Global Ecosystems Database, version 1.0, Disc A, NOAA National Geophysical Data Center, Boulder, Colorado, 1992.

Pantillon, F., Knippertz, P., Marsham, J. H., and Birch, C. E.: A Parameterization of Convective Dust Storms for Models with Mass-Flux Convection Schemes, Journal of the Atmospheric Sciences, 72, 2545–2561, doi:10.1175/JAS-D-14-0341.1, 2015.

Pantillon, F., Knippertz, P., Marsham, J. H., Panitz, H.-J., and Bischoff-Gauss, I.: Modeling haboob dust storms in large-scale weather and climate models, Journal of Geophysical Research: Atmospheres, 121, 2090–2109, doi:10.1002/2015JD024349, 2016.

Pérez, C., Nickovic, S., Baldasano, J. M., Sicard, M., Rocadenbosch, F., and Cachorro, V. E.: A long Saharan dust event over the western Mediterranean: Lidar, Sun photometer observations, and regional dust modeling, Journal of Geophysical Research: Atmospheres, 111, n/a–n/a, doi:10.1029/2005JD006579, http://dx.doi.org/10.1029/2005JD006579, d15214, 2006.

Popp, T., de Leeuw, G., Bingen, C., Brühl, C., Capelle, V., Chedin, A., Clarisse, L., Dubovik, O., Grainger, R., Griesfeller, J., Heckel, A., Kinne, S., Klüser, L., Kosmale, M., Kolmonen, P., Lelli, L., Litvinov, P., Mei, L., North, P., Pinnock, S., Povey, A., Robert, C., Schulz, M., Sogacheva, L., Stebel, K., Stein Zweers, D., Thomas, G., Tilstra, L., Vandenbussche, S., Veefkind, P., Vountas, M., and Xue, Y.: Development, Production and Evaluation of Aerosol Climate Data Records from European Satellite Observations (Aerosol_cci), Remote Sensing, 8, 421–, doi:10.3390/rs8050421, 2016.

Pozzer, A., de Meij, A., Yoon, J., Tost, H., Georgoulias, A. K., and Astitha, M.: AOD trends during 2001–2010 from observations and model simulations, Atmospheric Chemistry and Physics, 15, 5521–5535, doi:10.5194/acp-15-5521-2015, 2015.

Pringle, K. J., Tost, H., Message, S., Steil, B., Giannadaki, D., Nenes, A., Fountoukis, C., Stier, P., Vignati, E., and Lelieveld, J.: Description and evaluation of GMXe: a new aerosol submodel for global simulations (v1), Geoscientific Model Development, 3, 391, doi:10.5194/gmd-3-391-2010, 2010a.

Pringle, K. J., Tost, H., Metzger, S., Steil, B., Giannadaki, D., Nenes, A., Fountoukis, C., Stier, P., Vignati, E., and Lelieveld, J.: Corrigendum to "Description and evaluation of GMXe: a new aerosol submodel for global simulations (v1)" published in Geosci. Model Dev., 3, 391-412, 2010, Geoscientific Model Development, 3, 413, doi:10.5194/gmd-3-413-2010, 2010b.

Sayer, A. M., Munchak, L. A., Hsu, N. C., Levy, R. C., Bettenhausen, C., and Jeong, M.-J.: MODIS Collection 6 aerosol products: Comparison between Aqua's e-Deep Blue, Dark Target, and "merged" data sets, and usage recommendations, Journal of Geophysical Research: Atmospheres, 119, 13,965–13,989, doi:10.1002/2014JD022453, 2014.

Scholes, R. and Brown de Colstoun, E.: ISLSCP II Global Gridded Soil Characteristics, in: ISLSCP Initiative II Collection, edited by Hall, F. G., Collatz, G., Meeson, B., Los, S., de Colstoun, E. B., and Landis, D., ORNL Distributed Active Archive Center, doi:10.3334/ORNLDAAC/1004, http://dx.doi.org/10.3334/ORNLDAAC/1004, 2011.

Shangguan, W., Dai, Y., Duan, Q., Liu, B., and Yuan, H.: A global soil data set for earth system modeling, Journal of Advances in Modeling Earth Systems, 6, 249–263, doi:10.1002/2013MS000293, http://dx.doi.org/10.1002/2013MS000293, 2014.

Shao, Y.: A model for mineral dust emission, Journal of Geophysical Research: Atmospheres, 106, 20 239–20 254, doi:10.1029/2001JD900171, 2001.

Shao, Y., Wyrwoll, K.-H., Chappell, A., Huang, J., Lin, Z., McTainsh, G. H., Mikami, M., Tanaka, T. Y., Wang, X., and Yoon, S.: Dust cycle: An emerging core theme in Earth system science, Aeolian Research, 2, 181–204, doi:10.1016/j.aeolia.2011.02.001, 2011.

Shi, M., Yang, Z.-L., Stenchikov, G. L., Parajuli, S. P., Tao, W., and Kalenderski, S.: Quantifying the impacts of landscape heterogeneity and model resolution on dust emissions in the Arabian Peninsula, Environmental Modelling & Software, 78, 106–119, doi:10.1016/j.envsoft.2015.12.021, 2016.

Solomos, S., Ansmann, A., Mamouri, R.-E., Binietoglou, I., Patlakas, P., Marinou, E., and Amiridis, V.: Remote sensing and modeling analysis of the extreme dust storm hitting Middle East and Eastern Mediterranean in September 2015, Atmospheric Chemistry and Physics Discussions, 2016, 1–31, doi:10.5194/acp-2016-1006, http://www.atmos-chem-phys-discuss.net/acp-2016-1006/, 2016.

Solomos, S., Ansmann, A., Mamouri, R.-E., Binietoglou, I., Patlakas, P., Marinou, E., and Amiridis, V.: Remote sensing and modelling analysis of the extreme dust storm hitting the Middle East and eastern Mediterranean in September 2015, Atmospheric Chemistry and Physics, 17, 4063–4079, doi:10.5194/acp-17-4063-2017, https://www.atmos-chem-phys.net/17/4063/2017/, 2017.

Spyrou, C., Mitsakou, C., Kallos, G., Louka, P., and Vlastou, G.: An improved limited area model for describing the dust cycle in the atmosphere, Journal of Geophysical Research: Atmospheres, 115, n/a–n/a, doi:10.1029/2009JD013682, http://dx.doi.org/10.1029/2009JD013682, d17211, 2010.

Tanre, D., Geleyn, J.-F., and Slingo, J. M.: First results of the introduction of an advanced aerosol-radiation interaction in the ECMWF low resolution global model, in: Aerosols and their climatic effects, edited by Gerber, H. and Deepak, A., pp. 133–177, A. Deepak Pub., 1984.

Taylor, K. E.: Summarizing multiple aspects of model performance in a single diagram, Journal of Geophysical Research: Atmospheres, 106, 7183–7192, doi:10.1029/2000JD900719, 2001.

Tegen, I.: Impact of vegetation and preferential source areas on global dust aerosol: Results from a model study, Journal of Geophysical Research, 107, 4576, doi:10.1029/2001JD000963, 2002.

White, B. R.: Soil transport by winds on Mars, Journal of Geophysical Research, 84, 4643–4651, doi:10.1029/JB084iB09p04643, 1979.

Yuan, H., Dai, Y., Xiao, Z., Ji, D., and Shangguan, W.: Reprocessing the MODIS Leaf Area Index products for land surface and climate modelling, Remote Sensing of Environment, 115, 1171 – 1187, doi:http://dx.doi.org/10.1016/j.rse.2011.01.001, http://www.sciencedirect.com/science/article/pii/S0034425711000149, 2011.

Zender, C. S., Bian, H., and Newman, D.: Mineral Dust Entrainment and Deposition (DEAD) model: Description and 1990s dust climatology, Journal of Geophysical Research: Atmospheres, 108, n/a–n/a, doi:10.1029/2002JD002775, http://dx.doi.org/10.1029/2002JD002775, 4416, 2003.

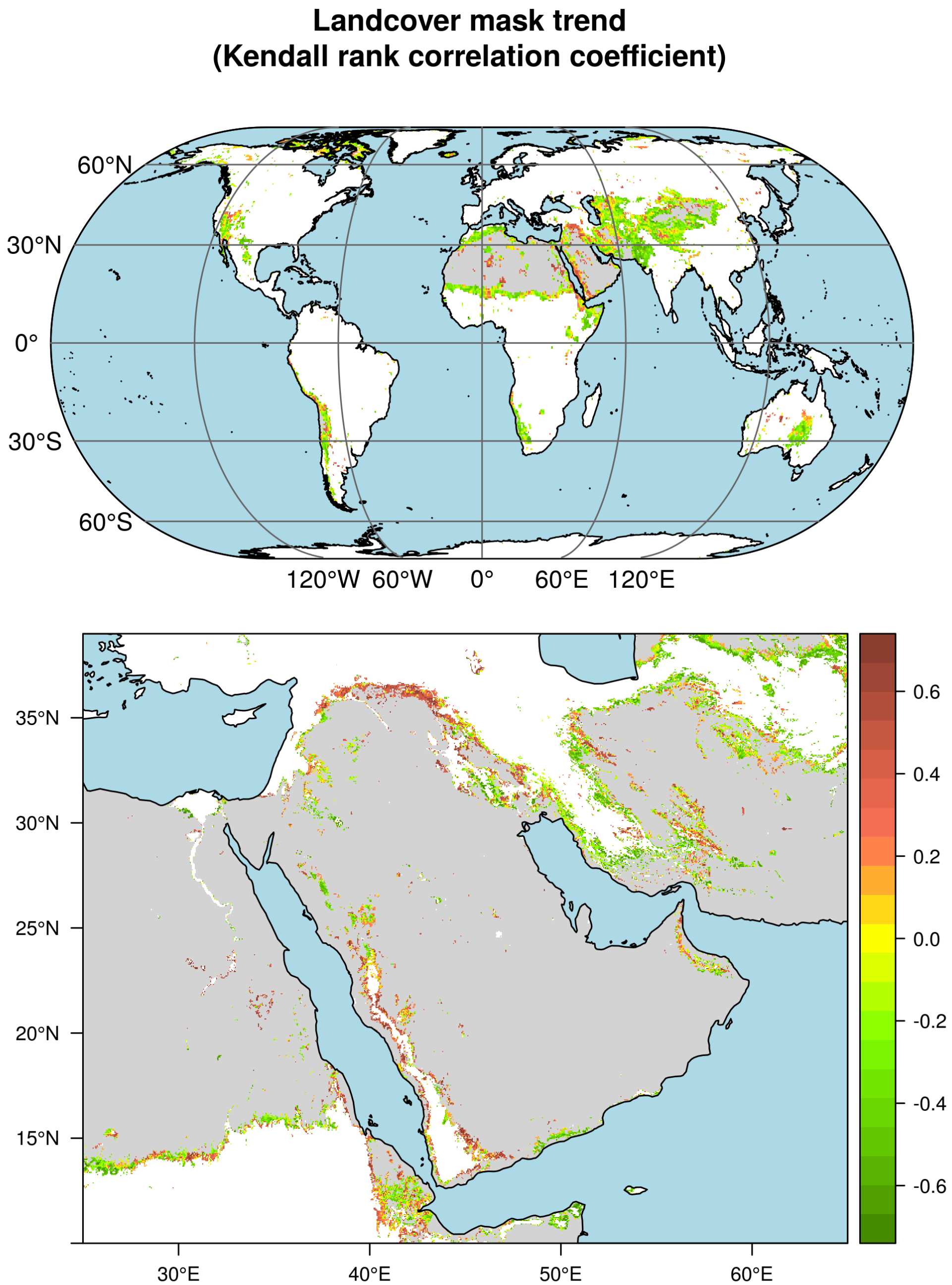

Figure 1. Trend of the dust emission mask based on the MODIS MCD12C1 landcover product during the period 2001 to 2012. Regions with changing surface properties are coloured according to the Kendall rank correlation coefficient τ of time and mask value, depicting expansion of source regions (i.e., positive correlation coefficients) in red, and contraction in green. Regions where the land cover remained unchanged are grey (source regions) or white (non-source regions). For better readability, in the global plot (top) the values have been averaged over 10 by 10 pixels ignoring constant pixels. The magnified plot of the Middle East (bottom) shows the original 0.05° pixels.

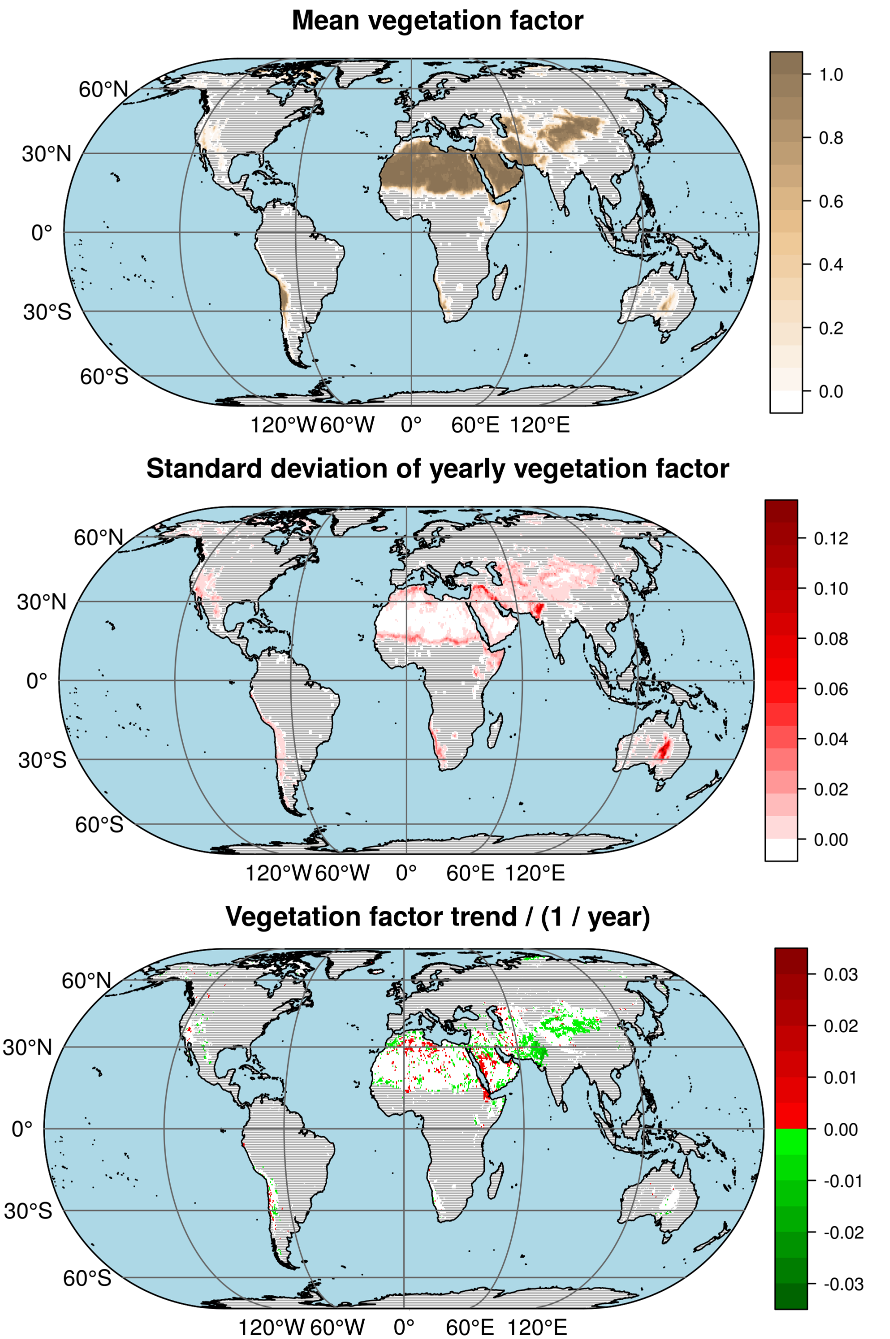

Figure 2. Vegetation factor based on leaf area index data from Yuan et al. (2011) averaged over the period 2000 to 2015 (top), the standard deviation of the annual mean values (center) and the trend of the annual mean values (bottom). Regions where the landcover mask precludes emissions throughout the period of available landcover data (2001 to 2012) are hatched.

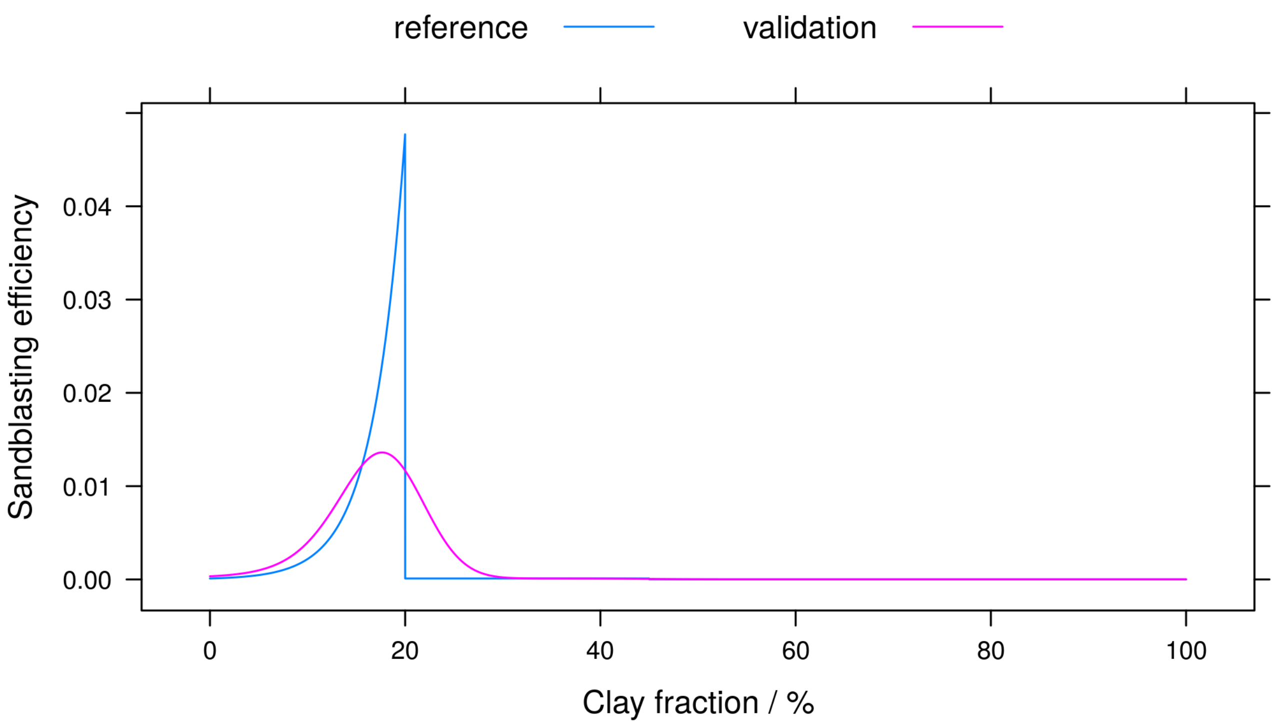

Figure 3. The sandblasting efficiency as function of the clay fraction used by Astitha et al. (2012), before ("reference") and after ("validation") applying a Gaussian filter with an interquartile range of 5 %.

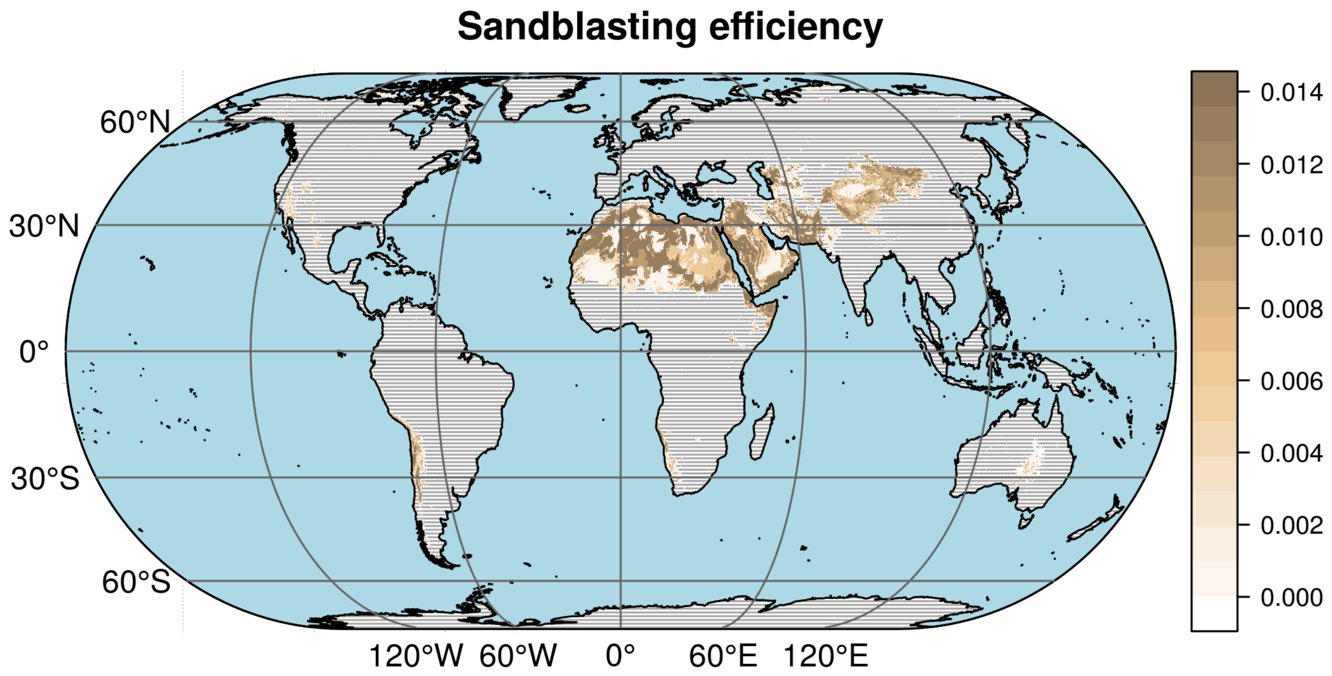

Figure 4. Global map of the sandblasting efficiency obtained by applying the filtered efficiency function shown in Fig. 3 to the GSDE clay fraction data. Regions where the landcover mask precludes emissions throughout the period of available landcover data (2001 to 2012) are hatched.

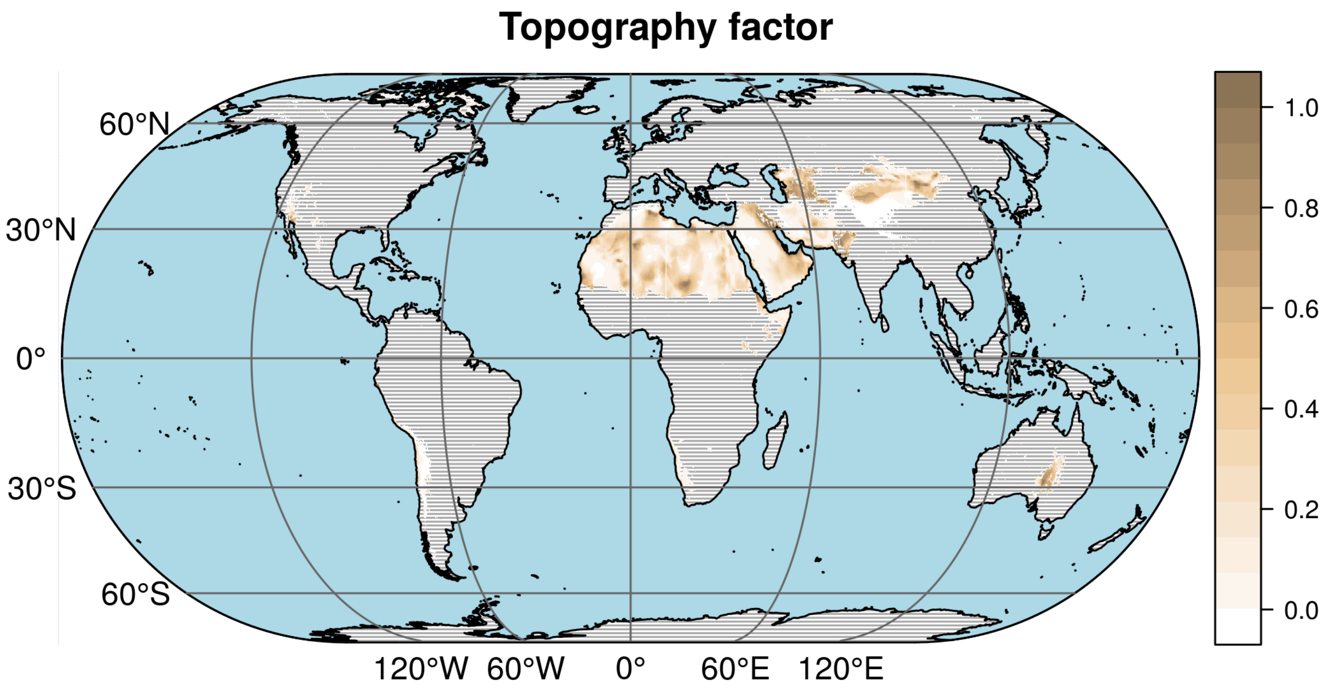

Figure 5. The topography factor defined by Eq. 3, calculated using the GMTED2010 elevation data. Regions where the landcover mask precludes emissions throughout the period of available landcover data (2001 to 2012) are hatched.

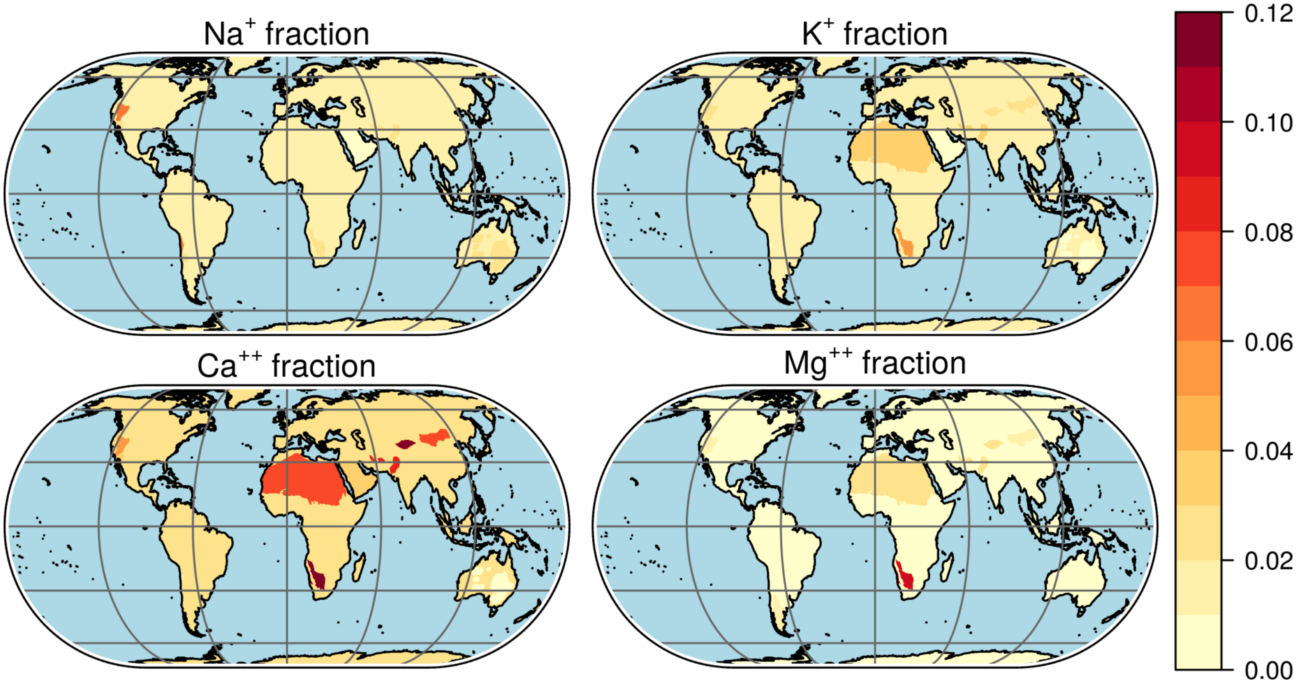

Figure 6. Maps of the Na^{+}, K^{+}, Ca^{++} and Mg^{++} mass fractions of the soil of different desert regions, used to calculate the chemical composition of the emitted dust particles.

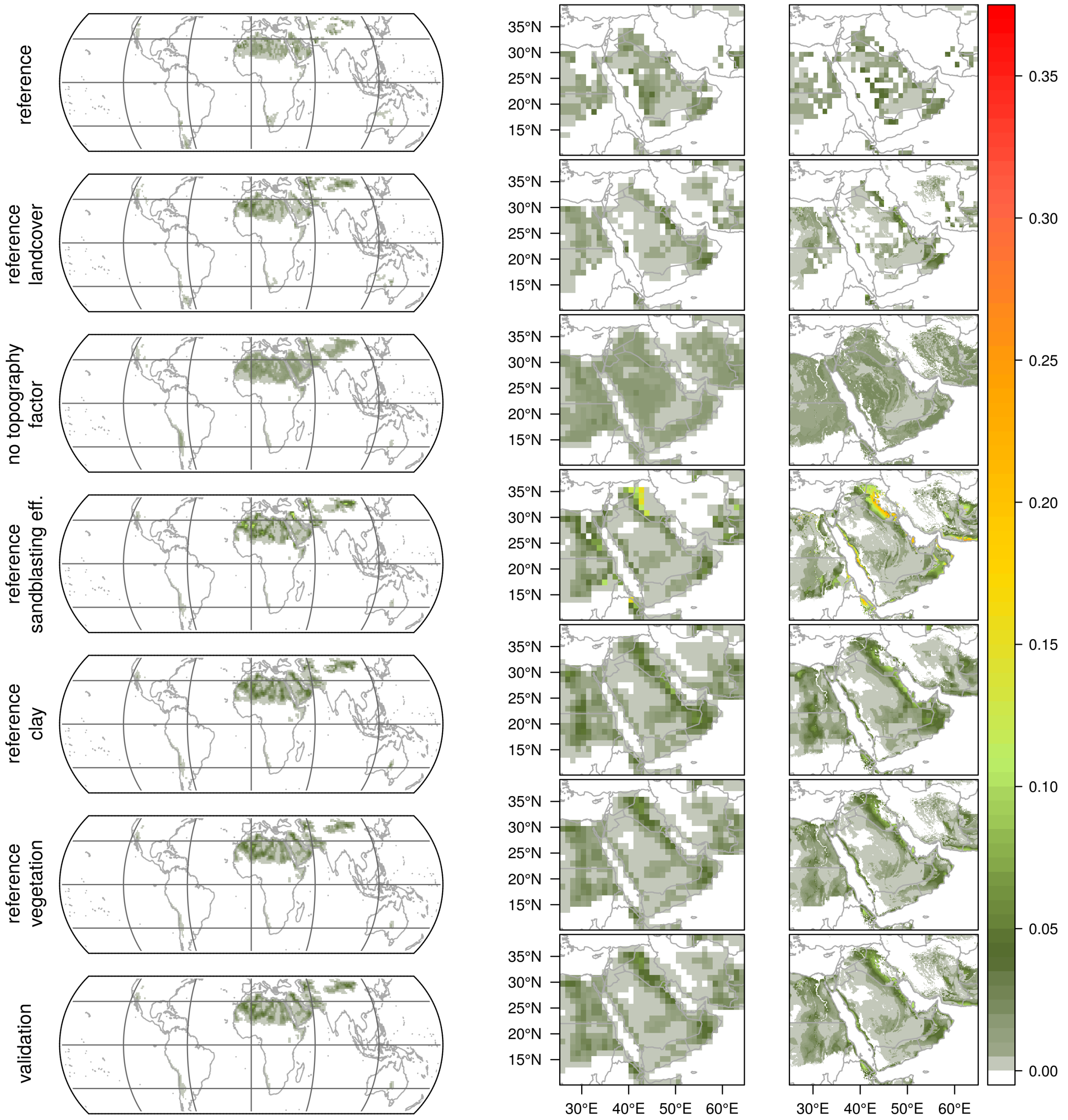

Figure 7. Distribution of the emission factor $a\ f_{\mathrm{landcover}}\ f_{\mathrm{veg}}\ N\ S_{\mathrm{topo}}$ during July 2011 for (from top to bottom) the original emission scheme, the revised emission scheme but using the reference landcover data, no topography factor, the reference sandblasting efficiency, clay fraction or vegetation, and the revised emissions. For the first and second column from the left all data have been regridded to T106 resolution, the third column showing the Middle East illustrates the effect of using the full resolution of the revised input data.

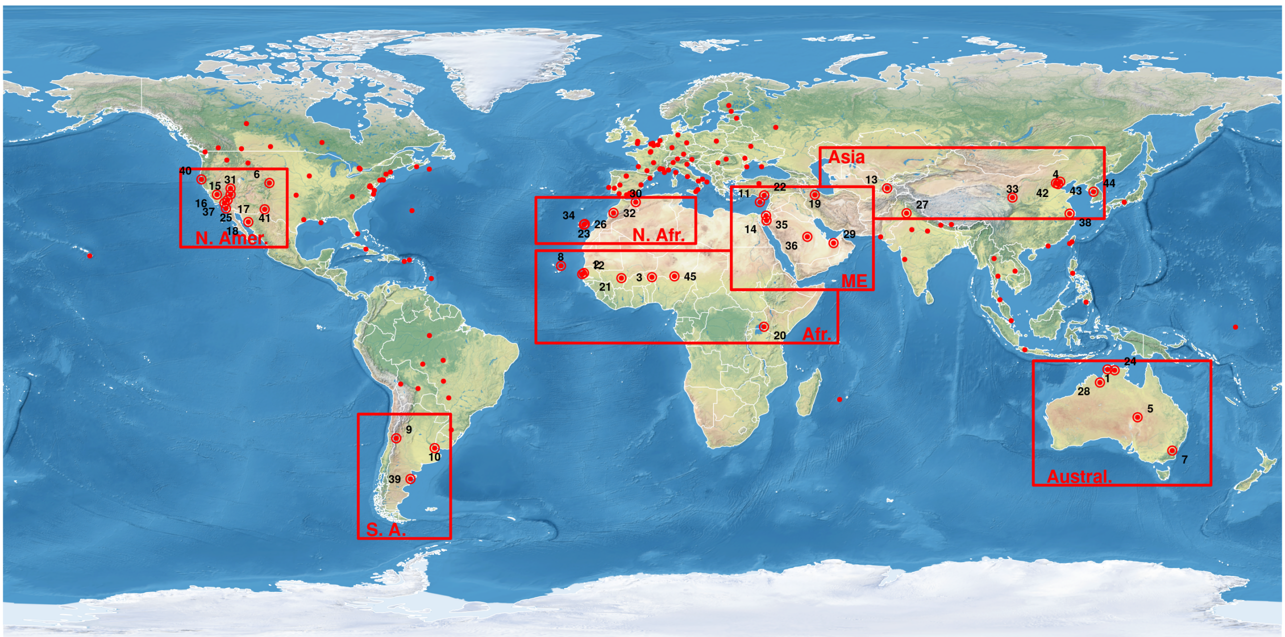

1 ARM_Darwin
2 Bambey-ISRA
3 Banizoumbou
4 Beijing
5 Birdsville
6 BSRN_BAO_Boulder
7 Canberra
8 Capo_Verde
9 CASLEO
10 CEILAP-BA
11 CUT-TEPAK
12 Dakar
13 Dushanbe
14 Eilat
15 Frenchman_Flat
16 Fresno
17 Goldstone
18 Hermosillo
19 IASBS
20 ICIPE-Mbita
21 IER_Cinzana
22 IMS-METU-ERDEMLI
23 Izana
24 Jabiru
25 La_Jolla
26 La_Laguna
27 Lahore
28 Lake_Argyle
29 Mezaira
30 Oujda
31 Railroad_Valley
32 Saada
33 SACOL
34 Santa_Cruz_Tenerife
35 SEDE_BOKER
36 Solar_Village
37 TABLE_MOUNTAIN_CA
38 Taihu
39 Trelew
40 Trinidad_Head
41 White_Sands_HELSTF
42 XiangHe
43 Xinglong
44 Yonsei_University
45 Zinder_Airport

Figure 8. AERONET stations and regions of interest ~~(A to F)~~ used for the evaluation. Stations with data for 120 or more days distributed over at least 9 months of 2011 (red dots) are considered, yielding 45 stations within the regions of interest (labelled).

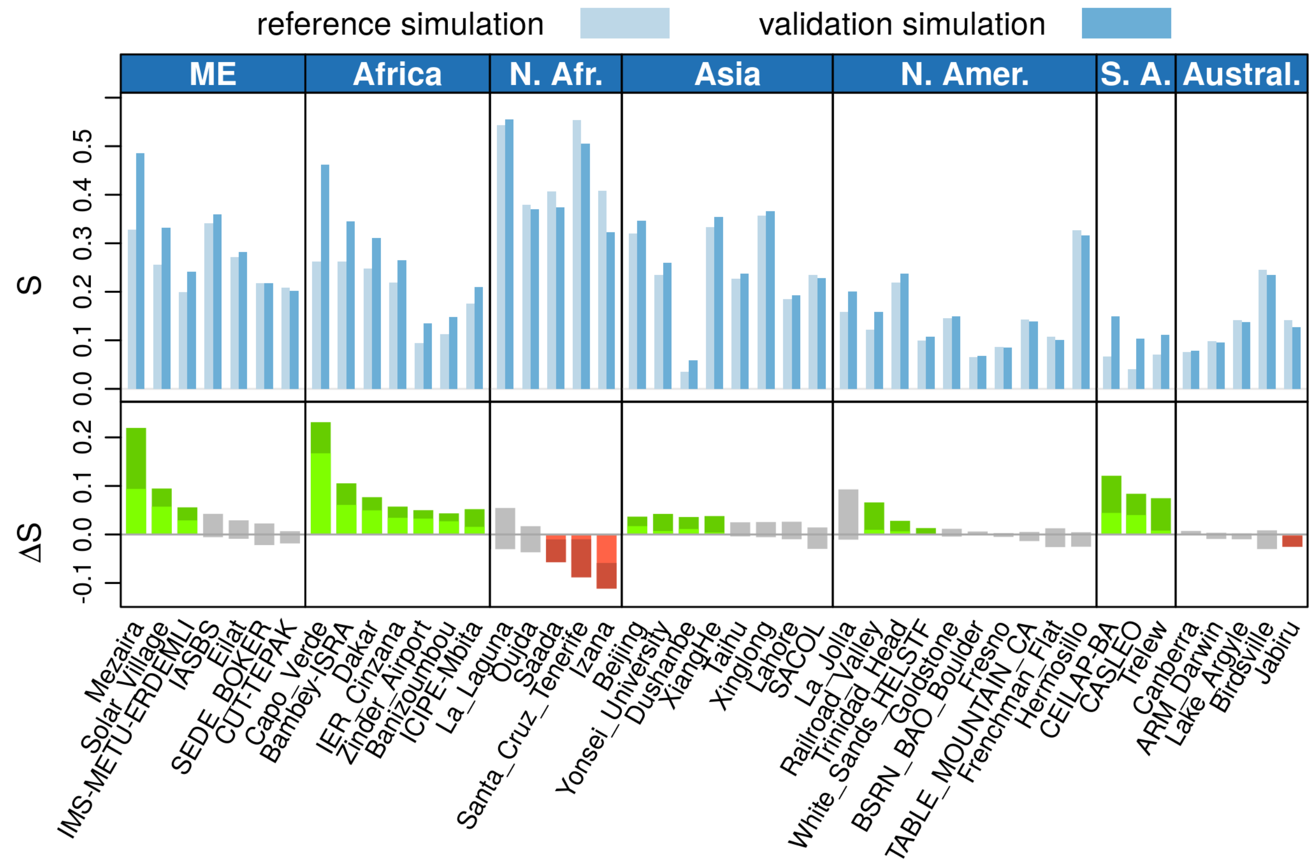

Figure 9. Skill score S of the daily mean 550 nm AOD from reference and validation simulations using AERONET observations as benchmark. The red~~and~~, green and grey bars depict the differences between reference and validation values, with green bars indicating that the validation results agree more closely with the measurements by at least one standard deviation σ. The corresponding error intervals are indicated by darker colours. Generally, the validation simulation performs better than the reference simulation; regarding the decreased skill scores in north-west Africa, please refer to the discussion in the main text.

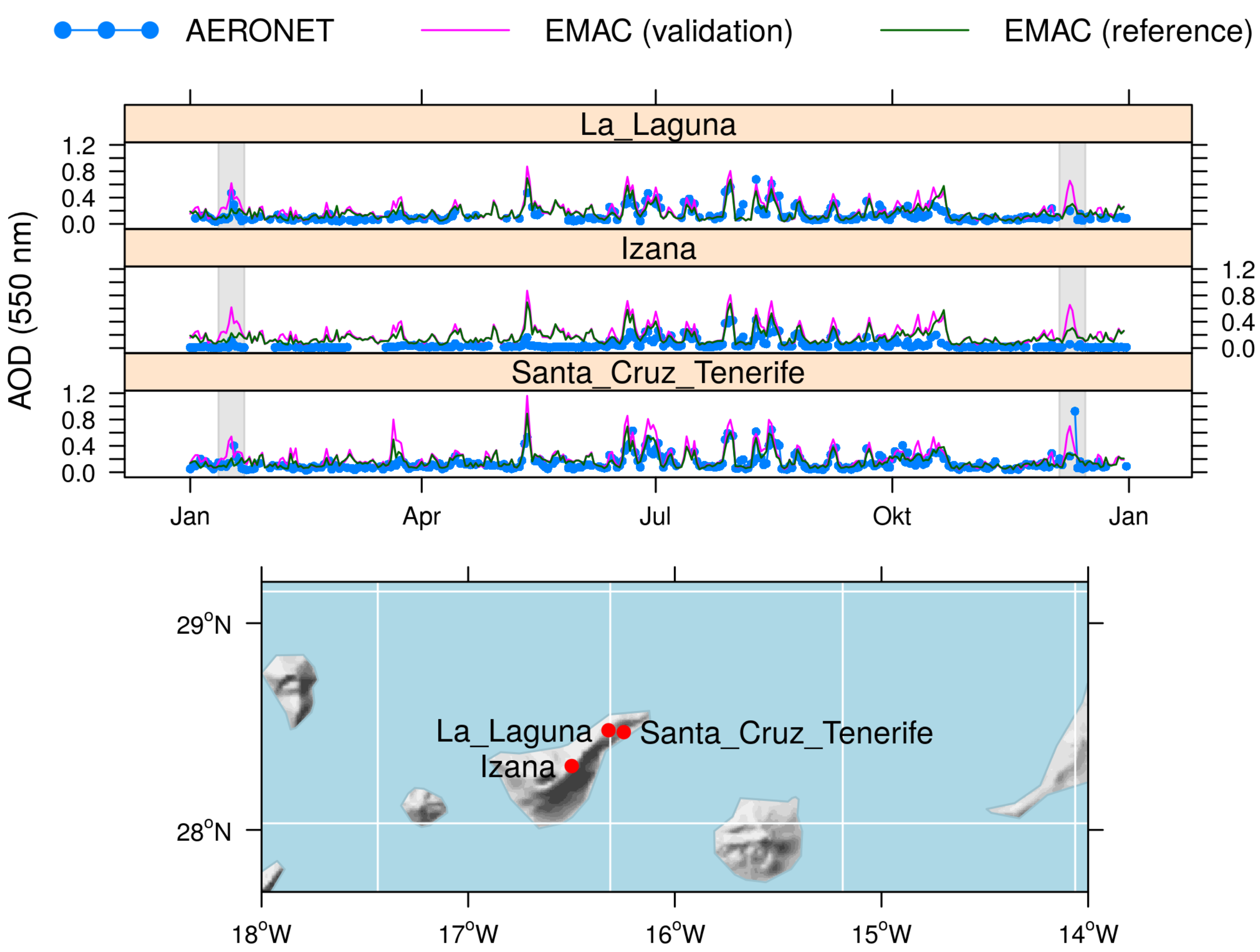

Figure 10. Time series of the daily mean AOD at the Canarian AERONET stations (top) and a map showing the location of the stations (bottom). The white ~~grid depicts~~ squares depict the T106 model grid. During the grey shaded periods of the time series in January and December, at least one of the three AERONET stations observed an AOD peak which is reproduced by the validation but not by the reference simulation.

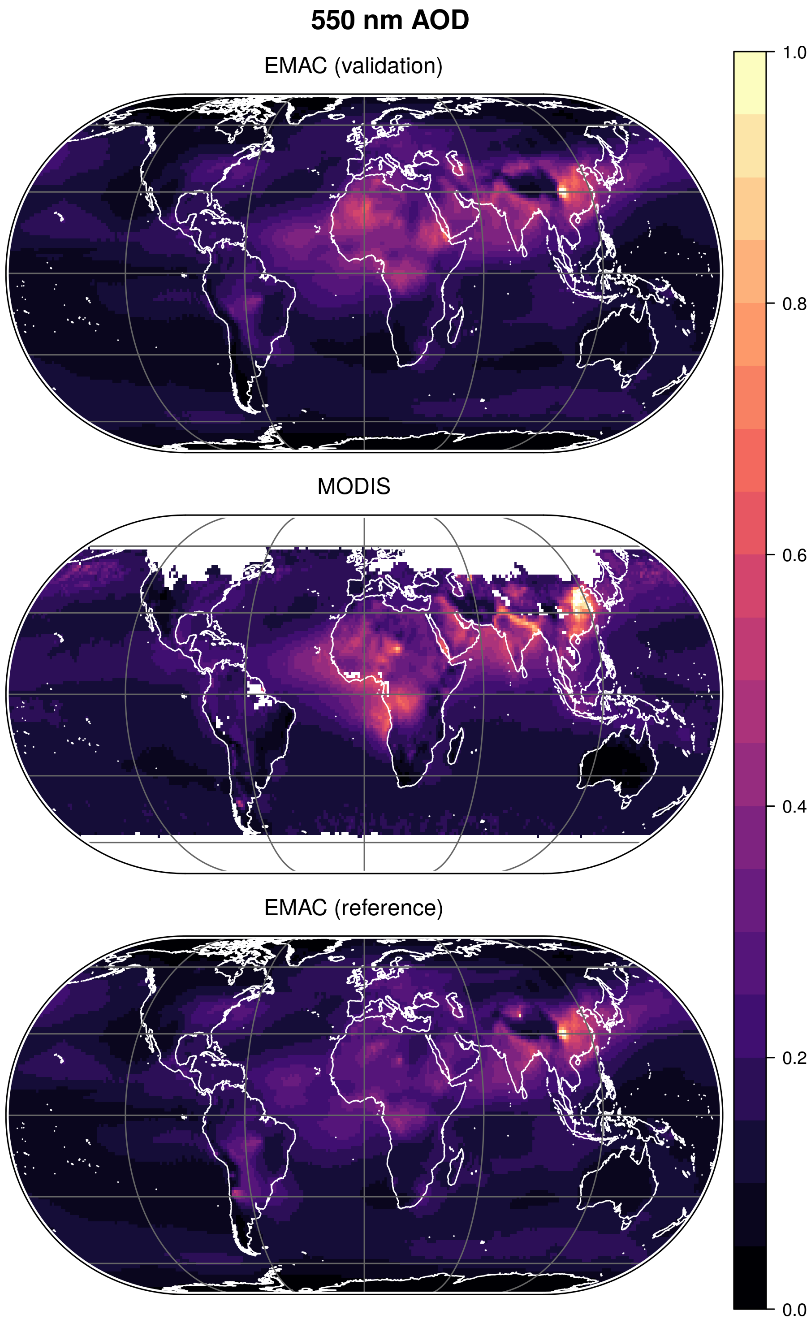

Figure 11. Annual mean for 2011 of the AOD at $550\ \mathrm{nm}$ wavelength observed by MODIS (centre) and simulated by EMAC with ("validation", top) and without ("reference", bottom) revision of the dust emission scheme. The revised dust emissions enhance the correlation of the AOD pattern from 0.79 to 0.81, the skill score from 0.58 to 0.67.

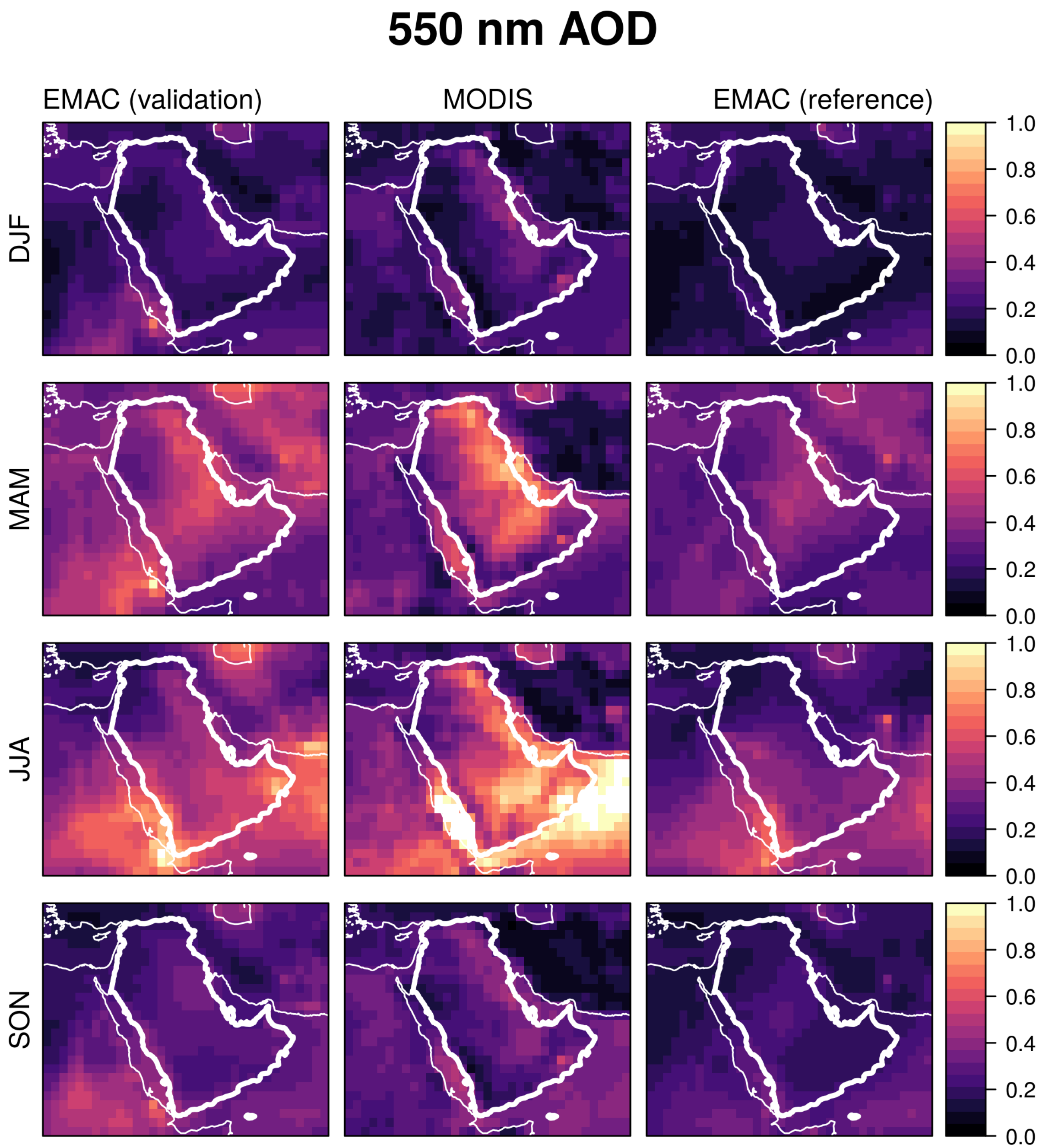

Figure 12. Seasonal 550 nm AOD over the Middle East (region of interest A) in 2011 observed by MODIS (centre column) and simulated by EMAC with ("validation", left) and without ("reference", right) revision of the dust emission scheme. Each row shows the three-month averages over the periods (from top to bottom) DJF (December, January, February), MAM (March, April, May), JJA (June, July, August) and SON (September, October, November). Especially throughout the white-bounded region encompassing the Arabian Peninsula including Iraq, Syria and Jordan the AOD distribution obtained with the revised dust emissions agrees significantly better with the MODIS observations (see Fig. S6 in the supplement).

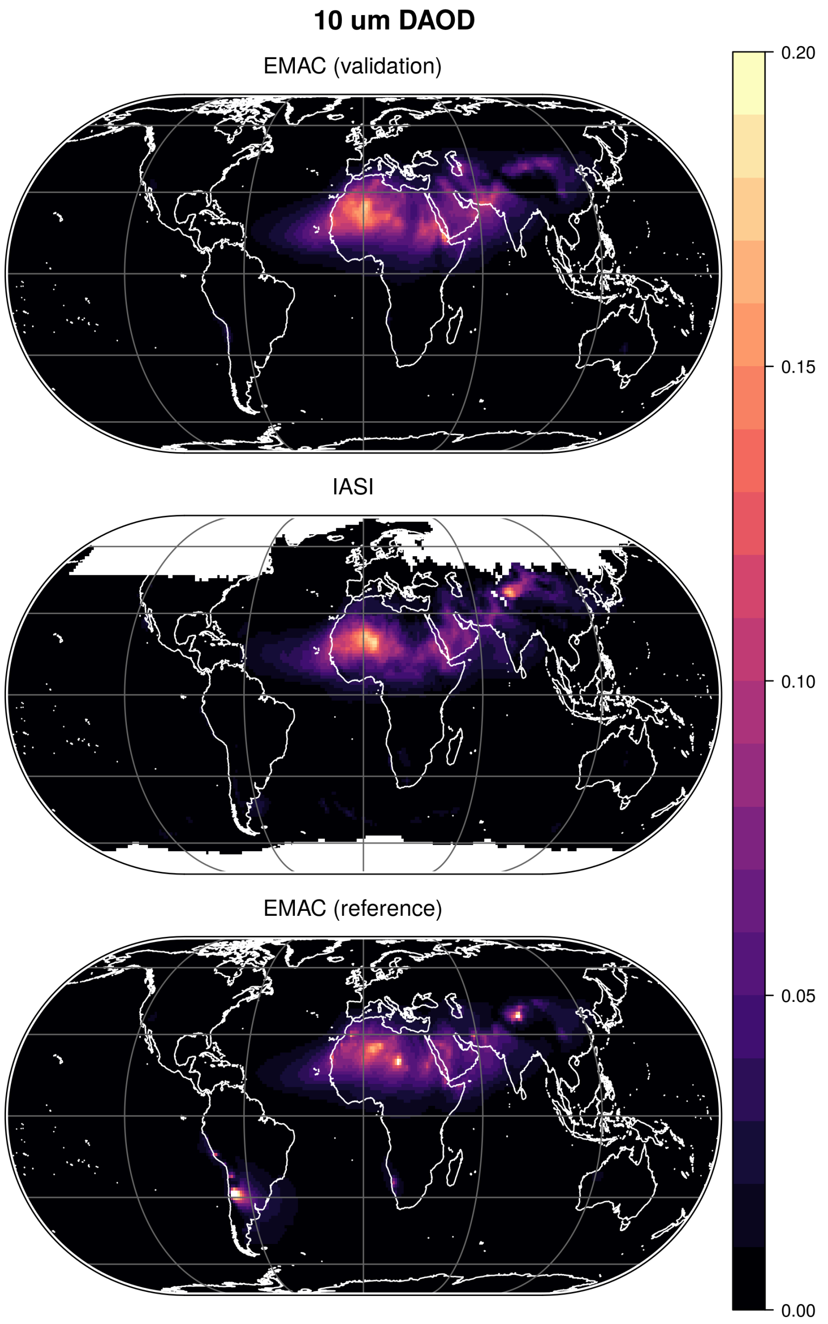

Figure 13. Annual mean for 2011 of the DAOD at 10 μm wavelength observed by IASI (centre) and simulated by EMAC with ("validation", top) and without ("reference", bottom) revision of the dust emission scheme. The revised dust emissions enhance the correlation of the AOD pattern from 0.79 to 0.89, the skill score from 0.64 to 0.78.

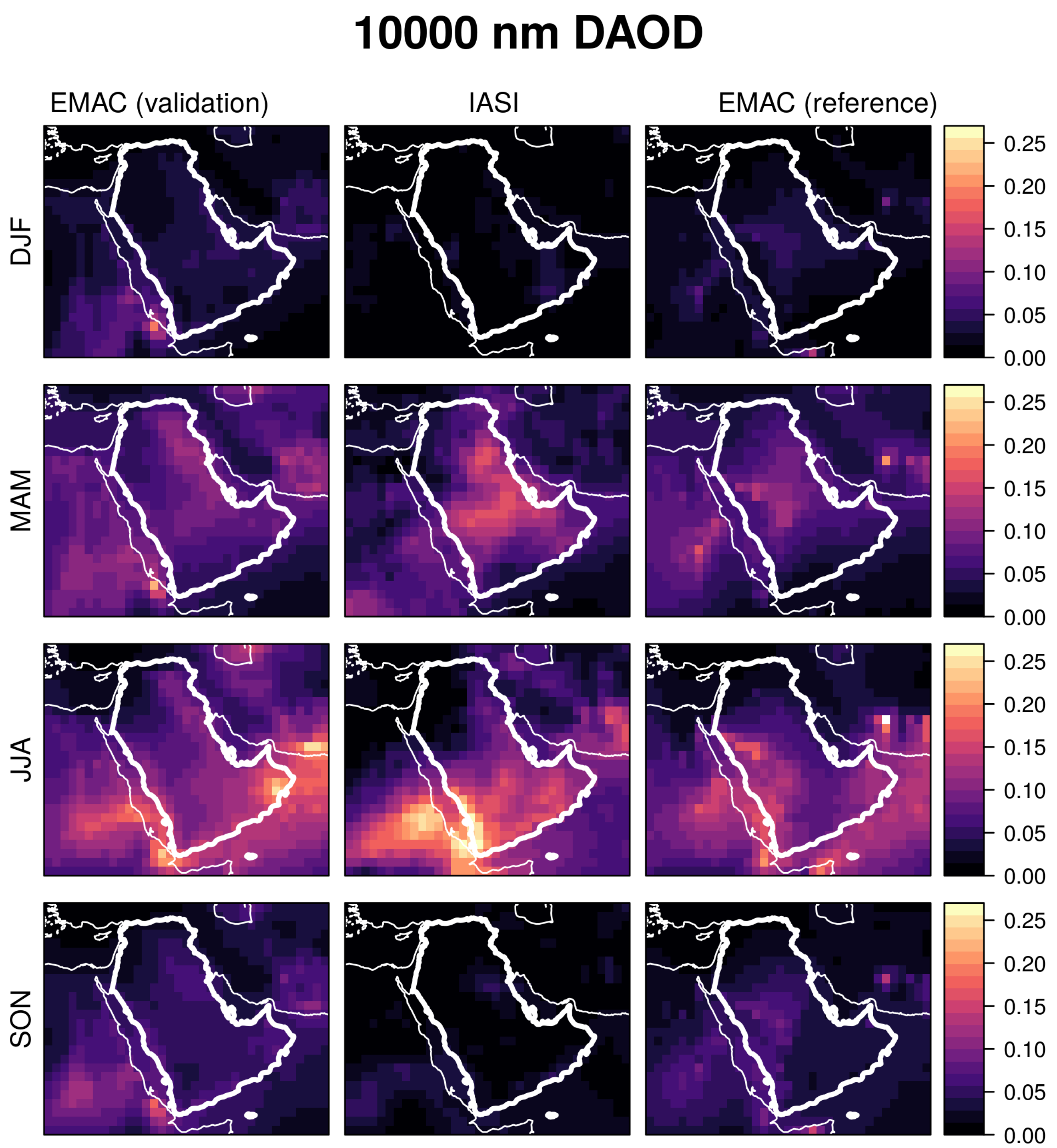

Figure 14. Seasonal 10 μm DAOD over the Middle East (region of interest A) in 2011 observed by IASI (centre column) and simulated by EMAC with ("validation", left) and without ("reference", right) revision of the dust emission scheme. Each row shows the three-month averages over the periods (from top to bottom) DJF (December, January, February), MAM (March, April, May), JJA (June, July, August) and SON (September, October, November). Especially throughout the white-bounded region encompassing the Arabian Peninsula including Iraq, Syria and Jordan the DAOD distribution obtained with the revised dust emissions agrees significantly better with the IASI observations (see Fig. S7 in the supplement).

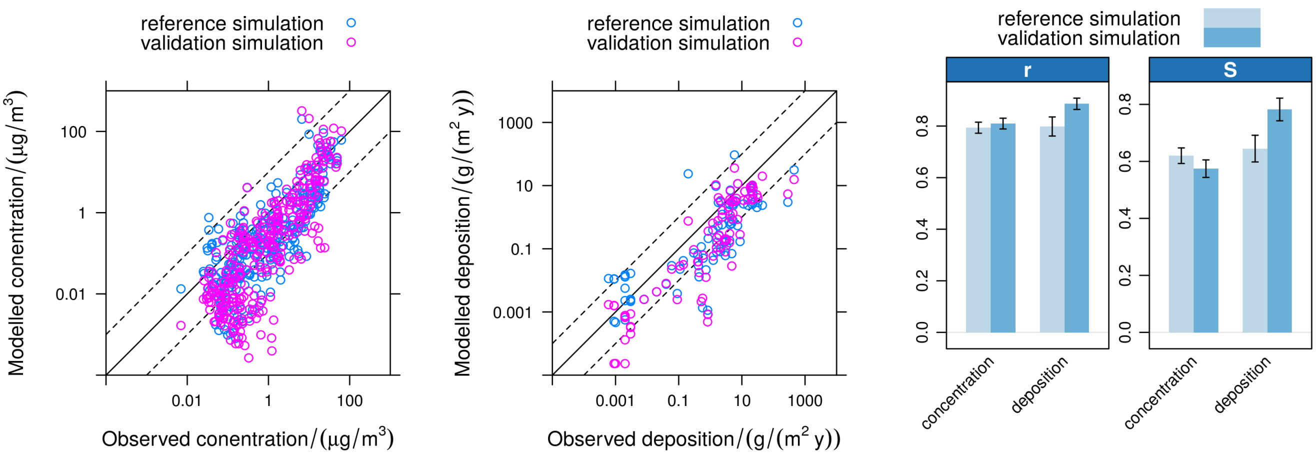

Figure 15. Comparison of modelled and observed dust concentration and deposition: scatterplots of monthly concentrations (left) and annual deposition (centre), and barcharts of the corresponding correlation coefficients r and skill scores S (right). The observations are taken from the AEROCOM dust benchmark (Huneeus et al., 2011).

Table 1. Summary of updated and added input data

		Reference input data	Updated/new input data
Land cover	Source	Olson (1992)	MODIS MCD12C1
	Spatial resolution	1°(aggregated from 10’)	0.05°
	Temporal resolution	static	yearly data (since 2001)
Clay fraction	Source	Scholes and Brown de Colstoun (2011)	GSDE (Shangguan et al., 2014)
	Spatial resolution	1°	0.1°(aggregated from 30")
	Temporal resolution	static	static
	Notes	clay fraction in top 30 cm soil layer	clay fraction in top 4.5 cm soil layer
Vegetation	Source	Kergoat et al. (1999); Bonan et al. (2002)	Yuan et al. (2011)
	Spatial resolution	1°(aggregated from 0.5°)	0.1°(aggregated from 30")
	Temporal resolution	monthly values (Apr 1992 to Mar 1993)	monthly values (since 2000, aggregated from 8 day values)
	Notes		MODIS based
Topography	Source	-	Danielson and Gesch (2011); GMTED2010 (2010)
	Spatial resolution	-	0.1°(aggregated from 30")
	Temporal resolution	-	static
Chemical composition	Source	-	Karydis et al. (2016); Natural Earth (2016)
	Spatial resolution	-	0.1°
	Temporal resolution	-	static

Table 2. Parameters of emission and GMXE dust modes. The GMXE parameter values shown have been used for reference and validation simulation.

	σ_g	$\tilde{d}/\mu\mathrm{m}$	$d_{\mathrm{min}}/\mu\mathrm{m}$	$d_{\mathrm{max}}/\mu\mathrm{m}$
Emission modes	2.1	0.83		
	1.9	4.82		
	1.6	19.4		
GMXE dust modes	1.59		0.12	2
	2		2	∞

Table 3. Global mineral dust emissions in 2011 obtained by EMAC.

	Validation simulation	Reference simulation
Accumulation mode	0.148 Gt / year	0.0517 Gt / year
Coarse mode	1.16 Gt / year	1.28 Gt / year
Total	1.31 Gt / year	1.33 Gt / year